

Thermodynamics and Phase Transitions of Nonlinear Electrodynamics Black Holes in an Extended Phase Space

Peng Wang,^{*} Houwen Wu,[†] and Haitang Yang[‡]

Center for Theoretical Physics, College of Physical Science and Technology,

Sichuan University, Chengdu, 610064, China

Abstract

We investigate the thermodynamic behavior of nonlinear electrodynamics (NLED) black holes in an extended phase space, which includes the cosmological constant $\Lambda = -3/l^2$ and dimensionful couplings a in NLED as thermodynamic variables. For a generic NLED black hole with the charge Q , we find that the Smarr relation is satisfied in the extended phase space, and the state of equation can be written as $Tl = \tilde{T}(r_+/l, Q/l, al^{-c})$, where $[a] = L^c$, and T and r_+ are the temperature and horizon radius of the black hole, respectively. For some values of Q/l and al^{-c} , the phase structure of the black hole is uniquely determined. Focusing on Born-Infeld and iBorn-Infeld AdS black holes, we obtain the corresponding phase diagrams in the a/l^2 - Q/l plane, which provides a new viewpoint towards the black holes' phase structure and critical behavior. For Born-Infeld black holes, the critical line and the region, where a reentrant phase transition occurs, in the a/l^2 - Q/l plane are both finite and terminate at $\{\tilde{a}_c, \tilde{Q}_c\} \simeq \{0.069, 0.37\}$. However for iBorn-Infeld black holes, the critical line and the reentrant phase transition region in the a/l^2 - Q/l plane are semi-infinite and extend to $Q/l = \infty$. We also examine thermal and electrical stabilities of Born-Infeld and iBorn-Infeld AdS black holes.

^{*}Electronic address: pengw@scu.edu.cn

[†]Electronic address: iverwu@scu.edu.cn

[‡]Electronic address: hyanga@scu.edu.cn

Contents

I. Introduction	2
II. NLED Black Hole	5
A. Black Hole Solution	5
B. Euclidean Action Calculation	8
C. Thermodynamic	10
III. Born-Infeld AdS Black Hole	14
IV. iBorn-Infeld AdS Black Hole	23
V. Conclusion	32
Acknowledgments	33
A. Derivation of Smarr Relation	33
References	34

I. INTRODUCTION

Black holes are among the most intriguing concepts of general relativity, which could have a deep impact upon the understanding of quantum gravity. Understanding the statistical mechanics of black holes has been a subject of intensive study for several decades. In the pioneering work [1–3], Hawking and Bekenstein found that black holes possess the temperature and the entropy. Analogous to the laws of thermodynamics, the four laws of black hole mechanics were established in [4].

Studying the phase transitions of AdS black holes is primarily motivated by AdS/CFT correspondence [5]. Hawking and Page showed that a first-order phase transition occurs between Schwarzschild AdS black holes and thermal AdS space [6], which was later understood as a confinement/deconfinement phase transition in the context of the AdS/CFT correspondence [7]. For Reissner-Nordstrom (RN) AdS black holes, authors of [8, 9] showed that their critical behavior is similar to that of a Van der Waals liquid gas phase transition.

Later, the asymptotically AdS black holes have been studied in the context of extended phase space thermodynamics, where the cosmological constant is interpreted as thermodynamic pressure [10, 11]. In this case, the black hole mass should be understood as enthalpy instead of the internal energy [12]. The P - V criticality study has been explored for various AdS black holes [13–18]. It showed that the P - V critical behaviors of AdS black holes are similar to that of a Van der Waals liquid gas system. A reentrant phase transition occurs if, as one monotonically changes a thermodynamic variable, the system undergoes two (or more) phase transitions and returns to a state macroscopically similar to the initial state. In the context of the extended phase space, the reentrant phase transition has been observed for some AdS black holes, e.g., 4D BI-AdS black holes [19], higher dimensional singly spinning Kerr-AdS black holes [20], AdS black holes in Lovelock gravity [16], AdS black holes in dRGT massive gravity [21], hairy AdS black holes [22].

Nonlinear electrodynamics (NLED) is an effective model incorporating quantum corrections to Maxwell electromagnetic theory. Coupling NLED to gravity, various NLED charged black holes were derived and discussed in a number of papers [23–29]. The thermodynamics of NLED black holes in the extended phase space have been considered in literature, e.g., power Maxwell invariant black holes [30–32], non-linear magnetic-charged dS black hole [33].

Among the various NLED, there is a famous string-inspired one: Born-Infeld electrodynamics, which encodes the low-energy dynamics of D-branes. Born-Infeld electrodynamics incorporates maximal electric fields and smooths divergences of the electrostatic self-energy of point charges. The Born-Infeld AdS (BI-AdS) black hole solution was first obtained in [34, 35]. The thermodynamic behavior and phase transitions of BI-AdS black holes were studied in the canonical ensemble [36] and in the grand ensemble [37]. The critical behavior and thermodynamics of BI-AdS black holes in various gravities were also investigated in [38–46]. In the extended phase space, the thermodynamic phase structure and critical behavior of 4D and higher dimensional BI-AdS black holes were studied in [19, 47], respectively. In [48], the thermodynamics of 4D BI-AdS black holes has recently been discussed in the case, in which the charge of the black hole varies and the pressure is fixed. The reentrant phase transition has been observed in 4D BI-AdS black holes while there was no reentrant phase transition for the system of higher dimensional BI-AdS black holes. Although the properties of BI-AdS black holes are thoroughly investigated in literature, their electrical stabilities have been rarely reported.

Recently, a new type of NLED black holes, namely iBorn-Infeld AdS (iBI-AdS) black holes, have been considered in [49] as holographic models behaving as prototypes of Mott insulators. The Lagrangian of the iBorn-Infeld field can be obtained from that of the Born-Infeld field by extending the BI parameter (a in eqn. (57)) to a negative real number. In [50], it showed that the nonlinearity correction tends to reduce/increase the strength of the repulsive force between two electrons for the Born-Infeld/iBorn-Infeld field. So it is natural to expect that the iBI-AdS black hole is dual to a theory with strong interactions between electrons, which could lead to Mott-like behavior. Moreover, negative magneto-resistance and the Mott insulator to metal transition induced by a magnetic field can be realized at low temperatures in the iBorn-Infeld holographic models. Compared to the Born-Infeld case, the iBorn-Infeld case leads to a much richer transport behavior in the dual theory. As shown in [49], iBI-AdS black holes satisfy the constraints to ensure consistency in the form of ghostly perturbations and/or gradient instabilities at the decoupling limit. However, the thermodynamic behavior and phase structure of iBI-AdS black holes have yet to be discussed.

In this paper, we first investigate the thermodynamic behavior of generic NLED black holes in the extended phase space. Then, we turn to study the phase structure and critical behavior of BI-AdS and iBI-AdS black holes by studying the phase diagrams in the $Q/l-a/l^2$ plane. The rest of this paper is organized as follows. In section II, we derive the NLED black hole solution, compute its Euclidean action and discuss thermodynamic properties of the black hole. We find that the Smarr relation is satisfied after including dimensionful couplings in NLED in the extended phase space. In section III, we study the phase structure and critical behavior of BI-AdS black holes. The phase diagram for BI-AdS black holes in the $Q/l-a/l^2$ plane is given in FIG. 4, from which one can read the black hole's phase structure and critical behavior. We further explore thermal and electrical stabilities of BI-AdS black holes. In section IV, the phase structure and critical behavior of iBI-AdS black holes are investigated, which can be inferred from the phase diagram in the $Q/l-a/l^2$ plane, FIG. 10. We also study thermal and electrical stabilities of iBI-AdS black holes. We summarize our results in section V. In appendix, we present an alternative derivation of the Smarr relation for NLED black holes.

II. NLED BLACK HOLE

In this section, we first derive the asymptotically AdS black hole solution in the Einstein-NLED gravity. After its Gibbs free energy is obtained via calculating the Euclidean action, we then discuss the thermodynamic properties of the black hole, e.g., Smarr relation, stability.

A. Black Hole Solution

Consider a 4-dimensional model of gravity coupled to a nonlinear electromagnetic field A_μ with the action given by

$$S_{\text{Bulk}} = \int d^4x \sqrt{-g} [R - 2\Lambda + \mathcal{L}(s, a_i)], \quad (1)$$

where the cosmological constant $\Lambda = -\frac{3}{l^2}$, and we take $16\pi G = 1$ for simplicity. In the action (1), we assume that the generic NLED Lagrangian $\mathcal{L}(s, a_i)$ is a function of s and the parameters a_i , where we build an independent nontrivial scalar using $F_{\mu\nu} = \partial_\mu A_\nu - \partial_\nu A_\mu$ and none of its derivatives:

$$s = -\frac{1}{4} F^{\mu\nu} F_{\mu\nu}. \quad (2)$$

The parameters a_i characterize the effects of nonlinearity in the NLED. We also assume that the NLED Lagrangian would reduce to the Maxwell Lagrangian for small fields:

$$\mathcal{L}(s, a_i) \approx s. \quad (3)$$

Varying the action (1) with respect to g_{ab} and A_a , we find that the equations of motion are

$$\begin{aligned} R_{\mu\nu} - \frac{1}{2} R g_{\mu\nu} - \frac{3}{l^2} g_{\mu\nu} &= \frac{T_{\mu\nu}}{2}, \\ \nabla_\mu G^{\mu\nu} &= 0, \end{aligned} \quad (4)$$

where $T_{\mu\nu}$ is the energy-momentum tensor:

$$T_{\mu\nu} = g_{\mu\nu} \mathcal{L}(s, a_i) + \frac{\partial \mathcal{L}(s, a_i)}{\partial s} F_\mu{}^\rho F_{\nu\rho}, \quad (5)$$

and we define the auxiliary fields $G^{\mu\nu}$:

$$G^{\mu\nu} = -\frac{\partial \mathcal{L}(s, a_i)}{\partial F_{\mu\nu}} = \frac{\partial \mathcal{L}(s, a_i)}{\partial s} F^{\mu\nu}. \quad (6)$$

To construct a black hole solution with asymptotic AdS spacetime, we take the following ansatz for the metric and the NLED field

$$ds^2 = -f(r) dt^2 + \frac{dr^2}{f(r)} + r^2 (d\theta^2 + \sin^2 \theta d\phi^2),$$

$$A = A_t(r) dt. \tag{7}$$

The equations of motion then take the form:

$$-1 + f(r) - \frac{3r^2}{l^2} + r f'(r) = \frac{r^2}{2} [\mathcal{L}(s, a_i) + A'_t(r) G^{rt}], \tag{8}$$

$$2f'(r) - \frac{6r}{l^2} + r f''(r) = r \mathcal{L}(s, a_i), \tag{9}$$

$$[r^2 G^{rt}]' = 0, \tag{10}$$

where

$$s = \frac{A_t^2(r)}{2} \text{ and } G^{rt} = -\frac{\partial \mathcal{L}(s, a_i)}{\partial s} A'_t(r). \tag{11}$$

It can show that eqn. (9) can be derived from eqns. (8) and (10). Eqn. (10) leads to

$$G^{tr} = \frac{q}{r^2}, \tag{12}$$

where q is a constant. Via eqns. (11) and (12), $A'_t(r)$ is determined by

$$\mathcal{L}'\left(\frac{A_t^2(r)}{2}, a_i\right) A'_t(r) = \frac{q}{r^2}. \tag{13}$$

Moreover, integrating eqn. (9) leads to

$$f(r) = 1 - \frac{m}{r} + \frac{r^2}{l^2} - \frac{1}{2r} \int_r^\infty dr r^2 \left[\mathcal{L}\left(\frac{A_t^2(r)}{2}, a_i\right) - A'_t(r) \frac{q}{r^2} \right], \tag{14}$$

where m is a constant. For large values of r , one finds that

$$f(r) = 1 - \frac{m}{r} + \frac{r^2}{l^2} + \frac{q^2}{4r^2} + \mathcal{O}(r^{-4}), \tag{15}$$

which reduces to the behavior of a RN-AdS black hole. At the horizon $r = r_+$ where $f(r_+) = 0$, the Hawking temperature of the black brane is given by

$$T = \frac{f'(r_+)}{4\pi}. \tag{16}$$

Hence at $r = r_+$, eqn. (8) gives

$$T = \frac{1}{4\pi r_+} \left\{ 1 + \frac{3r_+^2}{l^2} + \frac{r_+^2}{2} \left[\mathcal{L}\left(\frac{A_t^2(r_+)}{2}, a_i\right) - A'_t(r_+) \frac{q}{r_+^2} \right] \right\}. \tag{17}$$

The charge Q of the black hole can be expressed in terms of the constants q . In fact, if we turn on the external current J^μ , the action would include an interaction term:

$$S_I = 4\pi \int d^4x \sqrt{-g} J^\mu A_\mu, \quad (18)$$

and hence the equation of motion for A_μ becomes

$$\nabla_\nu G^{\mu\nu} = 4\pi J^\mu. \quad (19)$$

The charge passing through a spacelike hypersurface Σ is given by

$$Q = - \int_\Sigma d^3x \sqrt{\gamma} \sigma_\mu J^\mu, \quad (20)$$

where γ_{ij} is the induced metric, and σ^μ is the unit normal vector of Σ . Using Stokes's theorem and eqn. (19), we can express the charge as a boundary integral:

$$Q = -\frac{1}{4\pi} \int_{\partial\Sigma} d^2x \sqrt{\tilde{\gamma}} n_\mu \sigma_\nu G^{\mu\nu}, \quad (21)$$

where $\partial\Sigma$ is the boundary of Σ , $\tilde{\gamma}_{ij}$ is the induced metric, and n_μ is the unit outward-pointing normal vector. For the metric in eqn. (7), Σ and $\partial\Sigma$ can be a constant- t hypersurface and a two-sphere at $r = \infty$, respectively. In this case, one has

$$\sigma_\mu = (-f^{1/2}, 0, 0, 0) \text{ and } n_\mu = (0, f^{-1/2}, 0, 0). \quad (22)$$

Thus, the charge of the black hole given by eqn. (21) becomes

$$Q = \frac{1}{4\pi} \int d\theta d\phi r^2 \sin\theta \frac{q}{r^2} = q, \quad (23)$$

where we use eqn. (12). The gauge potential measured with respect to the horizon is

$$\Phi = 4\pi \int_{r_+}^{\infty} A'_t(r) = 4\pi A_t(\infty), \quad (24)$$

where we fix the gauge field $A_t(r)$ at the horizon to be zero, i.e., $A_t(r_+) = 0$. The electrostatic potential Φ plays a role as the conjugated variable to Q in black hole thermodynamics.

For asymptotically AdS spaces, the mass may be extracted by comparison to a reference background, e.g., vacuum AdS. Similar to the charge of the black hole, the mass can also be determined by the Komar integral

$$M = 4 \int d\theta d\phi r^2 \sin\theta (\sigma_\mu n_\nu \nabla^\mu K^\nu) - M_{\text{AdS}}, \quad (25)$$

where $K^\mu = (1, 0, 0, 0)$ is the Killing vector associated with t , and M_{AdS} is Komar integral associated with K^μ for vacuum AdS space

$$M_{\text{AdS}} = 4 \int d\theta d\phi r^2 \sin\theta \left(\frac{r}{l^2}\right). \quad (26)$$

At spatial infinity, one can use eqn. (15) to calculate

$$\sigma_\mu n_\nu \nabla^\mu K^\nu = \frac{1}{2} f'(r) = \frac{m}{2r^2} + \frac{r}{l^2} + \mathcal{O}(r^{-3}). \quad (27)$$

So the mass of the black hole is

$$M = 8\pi m. \quad (28)$$

B. Euclidean Action Calculation

In the Euclidean path integral approach to quantum gravity [51, 52], one can identify the Euclidean path integral with the thermal partition function:

$$Z = \int \mathcal{D}g e^{-S^E(g)}.$$

In the semiclassical approximation, the dominant contribution to the path integral comes from the classical solution, and hence one has

$$Z \simeq e^{-S^E}. \quad (29)$$

Here, S^E is the on-shell action which is obtained by substituting the classical solution to the action. In asymptotically AdS spaces, S^E needs to be regulated to cancel the divergences coming from the asymptotic region. In the background-subtraction method, one can regularize S^E by subtracting a contribution from a reference background. In [53], the background-subtraction method was used to compute S^E for RN-AdS black holes. On the other hand, there is the counterterm subtraction method [54, 55], in which the action S^E is regularized in a background-independent fashion by adding a series of boundary counterterms to the action. Specifically, the Kounterterms method [56, 57] has been proposed as a regularization scheme for gravity in asymptotically AdS spaces. In [58], the Euclidean action was computed for black hole solutions of AdS gravity coupled to the Born-Infeld electrodynamics using the Kounterterms method.

We now follow the method in [58] to calculate the Euclidean action for the asymptotically AdS NLED black hole solution (7) in canonical ensemble, in which the temperature and charge of the black hole are fixed. The regularized action is then given by

$$S_R = S_{\text{Bulk}} + S_{\text{ct}} + S_{\text{surf}} \quad (30)$$

where the boundary terms are

$$S_{\text{ct}} = \frac{l^2}{4} \int d^3y B_3 \text{ and } S_{\text{surf}} = - \int d^3y \sqrt{\gamma} n_\nu G^{\mu\nu} A_\mu, \quad (31)$$

B_3 is the 2nd Chern form, and n^μ is the unit outward-pointing normal vector of the boundary. Since the asymptotically AdS spacetime has constant curvature in the asymptotic region, it showed in [58] that after including the boundary term S_{ct} , the action was stationary around the classical solution under arbitrary variations of the metric $g_{\mu\nu}$. To keep the charge of the black hole fixed instead of the potential, the boundary term S_{surf} has to be added. In fact, varying the action with respect to A_μ gives

$$\delta S_R = \text{EOM} - \int d^3y \sqrt{\gamma} n_\nu \delta G^{\mu\nu} A_\mu = \text{EOM} - \int d^3y \frac{\sqrt{h} n_r A_t}{r^2} \delta Q.$$

For the Euclidean continuation of the action $S^E = iS_R$, the horizon at $r = r_+$ is shrunk to a point, and the manifold spans between $r = r_+$ and $r = \infty$. To avoid a conical singularity at the origin of the radial coordinate, one requires to identify the Euclidean time $\tau = -it$ as $\tau \sim \tau + \beta$, where the period $\beta = T^{-1}$ is the inverse of the Hawking temperature T . The Euclidean continuation of the counter term S_{ct} was calculated in [58]:

$$S_{\text{ct}}^E = -4\pi\beta l^2 f'(r) [f(r) - 1] |_{r=\infty}. \quad (32)$$

The bulk action is

$$S_{\text{Bulk}}^E = - \int_0^\beta d\tau \int d\Omega \int_{r_+}^\infty dr r^2 \left[R + \frac{6}{l^2} + \mathcal{L}(s, a_i) \right] = 4\pi\beta [r^2 f'(r)] |_{r_+}^\infty - \beta q\Phi, \quad (33)$$

where we use eqns. (9) and (24). The boundary term S_{surf}^E is

$$S_{\text{surf}}^E = \int_0^\beta d\tau \int d\Omega f^{1/2}(r) r^2 \sin\theta (n_\nu G^{\mu\nu} A_\mu) |_{r=\infty} = \beta q\Phi, \quad (34)$$

where we use eqn. (24), $f(r) \rightarrow 1$ as $r \rightarrow \infty$, and $n_\mu = (0, f^{-1/2}, 0, 0)$. To sum up all terms, the Euclidean action S^E is given by

$$S^E = -16\pi^2 r_+^2 + 4\pi\beta \{ r^2 f'(r) - l^2 f'(r) [f(r) - 1] \} |_{r=\infty} = \beta (M - TS), \quad (35)$$

where the entropy of the black hole is

$$S = 16\pi^2 r_+^2, \quad (36)$$

and eqn. (15) gives

$$\lim_{r \rightarrow \infty} \{r^2 f'(r) - l^2 f'(r)[f(r) - 1]\} = 2m. \quad (37)$$

Since the Euclidean action is calculated at fixed Q , $P (= 6/l^2)$ and T , we can associate it with the Gibbs free energy:

$$F = M - TS. \quad (38)$$

C. Thermodynamic

Here, we study the thermodynamics of the NLED AdS black hole solution in the extended phase space. In such perspective on black hole thermodynamics, one needs to include the cosmological constant Λ as a pressure term and interpret the mass of the black hole as a gravitational version of chemical enthalpy. Furthermore, as noted in Lovelock gravity [59] and Born-Infeld electrodynamics [19], any dimensionful coupling should be promoted to a thermodynamic variable and hence introduce the associated conjugate, which would add an extra term in the first law and Smarr relation.

In terms of the horizon radius r_+ , the mass M can be written as

$$M = 8\pi \left\{ r_+ + \frac{r_+^3}{l^2} - \frac{1}{2} \int_{r_+}^{\infty} dr r^2 \left[\mathcal{L} \left(\frac{A_t^2(r)}{2}, a_i \right) - A_t'(r) \frac{Q}{r^2} \right] \right\}. \quad (39)$$

So the derivatives of the mass in terms of the entropy and the charge are, respectively,

$$\frac{\partial M}{\partial S} = \frac{1}{4\pi r_+} \frac{\partial m}{\partial r_+} = T, \quad (40)$$

and

$$\frac{\partial M}{\partial Q} = 8\pi \left[-\frac{1}{2} \int_{r_+}^{\infty} dr r^2 \mathcal{L}' \left(\frac{A_t^2(r)}{2}, a_i \right) A_t'(r) \frac{\partial A_t'(r)}{\partial Q} + \frac{\Phi}{8\pi} + \frac{Q}{8\pi} \frac{\partial \Phi}{\partial Q} \right] = \Phi, \quad (41)$$

where we use eqns. (13) and (24). Since the pressure $P = 6/l^2$, one has

$$\frac{\partial M}{\partial P} = \frac{4\pi}{3} r_+^3 \equiv V, \quad (42)$$

where V is the thermodynamic volume. For dimensionful couplings a_i in $\mathcal{L}(s, a_i)$, we can introduce the associated conjugates \mathcal{A}_i :

$$\mathcal{A}_i = \frac{\partial M}{\partial a_i}. \quad (43)$$

Therefore, the extended first law takes the form

$$dM = TdS + VdP + \Phi dQ + \sum_i \mathcal{A}_i da_i. \quad (44)$$

Performing the dimensional analysis, we assume that $[a_i] = L^{c_i}$. The Euler scaling argument [60] gives the Smarr relation for the black holes

$$M = 2(TS - VP) + \sum_i c_i a_i \mathcal{A}_i + Q\Phi. \quad (45)$$

As a check, the Smarr relation are derived directly from the definitions of the thermodynamic quantities of the black hole in the appendix.

Till now, our expressions for the thermodynamics quantities, e.g., the Gibbs free energy F , the enthalpy M , are functions of the horizon radius r_+ (the entropy S), the charge Q and the pressure P (the AdS radius l). However, in canonical ensemble with fixed T , Q and P , we need to express the thermodynamics quantities in terms of T , Q and P . In doing so, the equation of state (17) is solved for r_+ : $r_+ = r_+(T, Q, P, a_i)$. Interestingly, the equation of state (17) can be rewritten as

$$\tilde{T} = \frac{1}{4\pi\tilde{r}_+} \left\{ 1 + 3\tilde{r}_+^2 + \frac{1}{2}\tilde{r}_+^2 \left[\mathcal{L} \left(\frac{\tilde{A}'_t(\tilde{r}_+)}{2}, \tilde{a}_i \right) - \tilde{A}'_t(\tilde{r}_+) \frac{\tilde{Q}}{\tilde{r}_+^2} \right] \right\}, \quad (46)$$

where we define

$$\tilde{T} = Tl, \quad \tilde{r}_+ = r_+/l, \quad \tilde{Q} = Q/l, \quad \tilde{a}_i = a_i l^{-c_i} \quad \text{and} \quad \tilde{A}'_t(r_+) = lA'_t(r_+), \quad (47)$$

and $\tilde{A}'_t(r_+)$ is determined by

$$\mathcal{L}' \left(\frac{\tilde{A}'_t(r_+)}{2}, \tilde{a}_i \right) \tilde{A}'_t(r_+) = \frac{\tilde{Q}}{\tilde{r}_+^2}. \quad (48)$$

Solving eqn. (46), we find that \tilde{r}_+ can be expressed as a function of \tilde{T} , \tilde{Q} and \tilde{a}_i : $\tilde{r}_+ = \tilde{r}_+(\tilde{T}, \tilde{Q}, \tilde{a}_i)$. With $\tilde{r}_+ = \tilde{r}_+(\tilde{T}, \tilde{Q}, \tilde{a}_i)$, we can express the thermodynamic quantities in terms of \tilde{T} , \tilde{Q} and \tilde{a}_i , e.g., the Gibbs free energy is given by

$$\tilde{F} \equiv F/l = \tilde{F}(\tilde{T}, \tilde{Q}, \tilde{a}_i).$$

The rich phase structure of the black hole comes from solving eqn. (46), i.e., $\tilde{T} = \tilde{T}(\tilde{r}_+, \tilde{Q}, \tilde{a}_i)$, for \tilde{r}_+ . If $\tilde{T}(\tilde{r}_+, \tilde{Q}, \tilde{a}_i)$ is a monotonic function with respect to \tilde{r}_+ for some

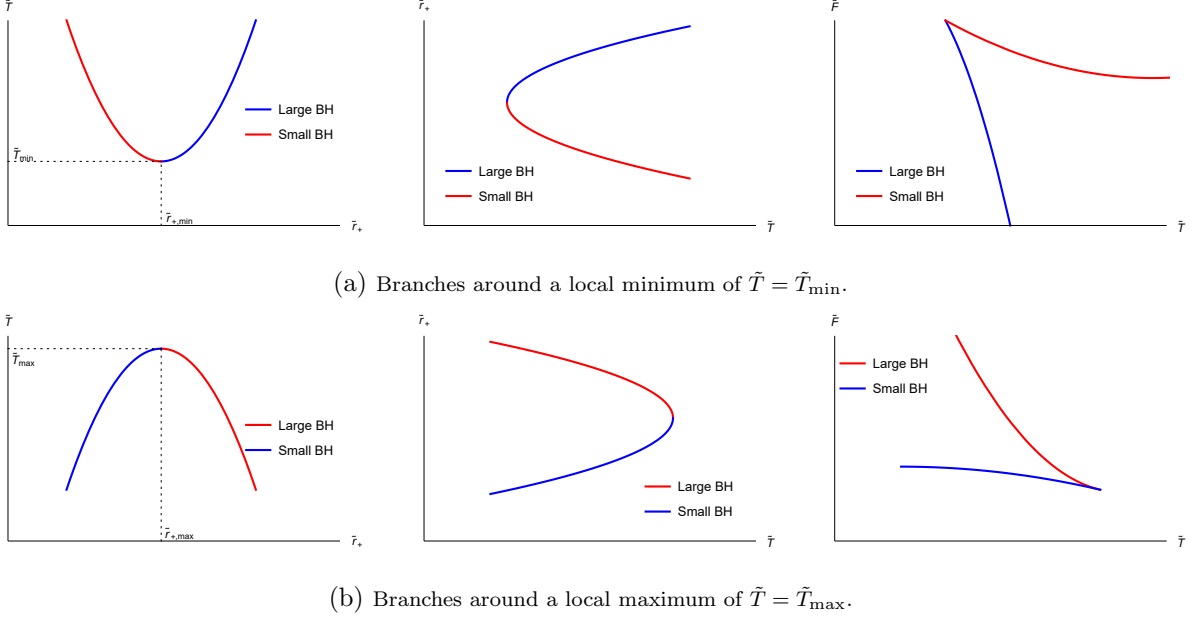


FIG. 1: Branches of black holes around local extremums of $\tilde{T} = \tilde{T}_{\min}$ and $\tilde{T} = \tilde{T}_{\max}$. Right panels: Gibbs free energy vs temperature. The blue branches are thermodynamically preferred and thermally stable. The red ones are thermally unstable. As $\tilde{T} \rightarrow \tilde{T}_{\max}/\tilde{T}_{\min}$, the red/blue branches become electrically stable/unstable.

values of \tilde{Q} and \tilde{a}_i , there would be only one branch for the black hole. More often, with fix \tilde{Q} and \tilde{a}_i , there exists a local minimum/maximum for $\tilde{T}(\tilde{r}_+, \tilde{Q}, \tilde{a}_i)$ at $\tilde{r}_+ = \tilde{r}_{+, \min}/\tilde{r}_+ = \tilde{r}_{+, \max}$. In this case, there are more than one branch for the black hole. In FIG. 1(a), we plot two branches, namely small BH and large BH, around a local minimum of $\tilde{T} = \tilde{T}_{\min}$. The Gibbs energy of these two branches is displayed in the right panel of FIG. 1(a). Since $\partial\tilde{F}(\tilde{T}, \tilde{Q}, \tilde{a}_i)/\partial\tilde{T} = -16\pi^2\tilde{r}_+^2$, the upper branch is small BH while lower one is large BH, which means that the large BH branch is thermodynamically preferred. Similarly, two branches around a local maximum of $\tilde{T} = \tilde{T}_{\max}$, small BH and large BH, are shown in FIG. 1(b). The upper/lower branch in the right panel of FIG. 1(b) is large/small BH since it has more/less negative slope. So the small BH branch is thermodynamically preferred in this case. In general, one might need to figure out how the existence of local extremums depend on values of \tilde{Q} and \tilde{a}_i to study the phase structure of the black hole.

After the black hole's branches are obtained, it is interesting to consider their thermodynamic stabilities against thermal and electrical fluctuations. In canonical ensemble, the

first quantity we consider is the specific heat at constant electric charge and pressure:

$$C_{Q,P} = T \left(\frac{\partial S}{\partial T} \right)_{Q,P} = 32l^2 \pi^2 \tilde{r}_+ \tilde{T} \frac{\partial \tilde{r}_+(\tilde{T}, \tilde{Q}, \tilde{a}_i)}{\partial \tilde{T}}. \quad (49)$$

Since the entropy is proportional to the size of the black hole, a positive specific heat means that the black hole radiate less when it is smaller. Thus, the thermal stability of the branch follows from $C_{Q,P} \geq 0$. From eqn. (49), it shows that the large/small BH branch in FIG. 1(a) and the small/large BH branch in FIG. 1(b) are both thermally stable/unstable. Note that $\partial^2 \tilde{F}(\tilde{T}, \tilde{Q}, \tilde{a}_i) / \partial^2 \tilde{T} = -l^{-2} C_{Q,P}$, and hence the thermally stable/unstable branches are concave downward/upward in right panels of FIG. 1.

The second quantity is

$$\epsilon_T = \left(\frac{\partial Q}{\partial \Phi} \right)_T = l \left[\frac{\partial \Phi(\tilde{r}_+, \tilde{Q}, \tilde{a}_i)}{\partial \tilde{Q}} - \frac{\partial \Phi(\tilde{r}_+, \tilde{Q}, \tilde{a}_i)}{\partial \tilde{r}_+} \frac{\frac{\partial \tilde{T}(\tilde{r}_+, \tilde{Q}, \tilde{a}_i)}{\partial \tilde{Q}}}{\frac{\partial \tilde{T}(\tilde{r}_+, \tilde{Q}, \tilde{a}_i)}{\partial \tilde{r}_+}} \right]^{-1}, \quad (50)$$

which describes how the black hole's electrostatic potential respond to its charge. Here, \tilde{r}_+ is understood as $\tilde{r}_+(\tilde{T}, \tilde{Q}, \tilde{a}_i)$. For a positive value of ϵ_T , as more charges are placed on the black hole, its potential increases and hence make it harder to move the system from equilibrium. The electrical stability of the branch then follows from $\epsilon_T \geq 0$. For the potential Φ , it is natural to expect that $\partial \Phi(\tilde{r}_+, \tilde{Q}, \tilde{a}_i) / \partial \tilde{r}_+ < 0$. We also assume $Q > 0$ and hence $\tilde{A}'_t(r_+) > 0$, which gives

$$\frac{\partial \tilde{T}(\tilde{r}_+, \tilde{Q}, \tilde{a}_i)}{\partial \tilde{Q}} = -\frac{1}{8\pi \tilde{r}_+} \tilde{A}'_t(r_+) < 0. \quad (51)$$

Eqn. (50) shows that in FIG. 1(a), $\epsilon_T^{-1} \rightarrow +\infty$ for the small BH branch and $\epsilon_T^{-1} \rightarrow -\infty$ for the large BH branch as $\tilde{T} \rightarrow \tilde{T}_{\min}$. Similarly in FIG. 1(b), $\epsilon_T^{-1} \rightarrow -\infty$ for the small BH branch and $\epsilon_T^{-1} \rightarrow +\infty$ for the large BH branch as $\tilde{T} \rightarrow \tilde{T}_{\max}$.

Finally, we turn to the critical point, which is an inflection point and obtained by

$$\frac{\partial \tilde{T}(\tilde{r}_+, \tilde{Q}, \tilde{a}_i)}{\partial \tilde{r}_+} = 0 \text{ and } \frac{\partial^2 \tilde{T}(\tilde{r}_+, \tilde{Q}, \tilde{a}_i)}{\partial \tilde{r}_+^2} = 0. \quad (52)$$

Solving the above equations gives

$$\tilde{r}_{+,c} = \tilde{r}_{+,c}(\tilde{a}_i), \quad \tilde{Q}_c = \tilde{Q}_c(\tilde{a}_i) \text{ and } \tilde{T}_c = \tilde{T}_c(\tilde{a}_i). \quad (53)$$

Defining the specific volume $v = \frac{r_+}{8\pi}$ [19], one finds that

$$\rho_c = \frac{P_c v_c}{T_c} = \frac{3}{4\pi} \frac{\tilde{r}_{+,c}(\tilde{a}_i)}{\tilde{T}_c(\tilde{a}_i)}. \quad (54)$$

Consider the case in which $\mathcal{L}(s, a_i)$ is a power series expansion of s :

$$\mathcal{L}(s, a_i) = s + \frac{a_1}{2}s^2 + \frac{a_2}{3}s^3 + \dots. \quad (55)$$

For small values of a_i , we find

$$\begin{aligned} \tilde{Q}_c &= \frac{1}{3} + \frac{7}{18}\tilde{a}_1 + \frac{11(\tilde{a}_1^2 + 16\tilde{a}_2)}{216} + \dots, \\ \tilde{T}_c &= \frac{1}{\pi} \sqrt{\frac{2}{3}} - \frac{\tilde{a}_1}{3\sqrt{6}\pi} - \frac{9\tilde{a}_1^2 + 32\tilde{a}_2}{36\sqrt{6}\pi} + \dots, \\ \tilde{r}_{+,c} &= \frac{1}{\sqrt{6}} - \frac{7\tilde{a}_1}{6\sqrt{6}} + \frac{27\tilde{a}_1^2 - 352\tilde{a}_2}{72\sqrt{6}} + \dots, \\ \rho_c &= \frac{P_c v_c}{T_c} = \frac{3(1 - \tilde{a}_1)}{8} + \frac{3\tilde{a}_1^2 - 40\tilde{a}_2}{24} + \dots. \end{aligned} \quad (56)$$

where

$$\tilde{Q}_c = Q_c \sqrt{P_c/6}, \tilde{T}_c = T_c \sqrt{6/P_c}, \tilde{r}_{+,c} = r_{+,c} \sqrt{P_c/6} \text{ and } \tilde{a}_i = (P_c/6)^i a_i.$$

The leading value of ρ_c is $3/8$, which reproduces the critical value ρ_c of RN-AdS black holes.

III. BORN-INFELD ADS BLACK HOLE

Born-Infeld electrodynamics is described by the Lagrangian density

$$\mathcal{L}(s) = \frac{1}{a} (1 - \sqrt{1 - 2as}), \quad (57)$$

where the coupling parameter a is related to the string tension α' as $a = (2\pi\alpha')^2 > 0$. When $a = 0$, we can recover the Maxwell Lagrangian. Solving eqn. (13) for $A'_t(r)$ gives

$$A'_t(r) = \frac{Q}{\sqrt{r^4 + aQ^2}}. \quad (58)$$

It follows that the potential of the black hole is

$$\Phi = \frac{4\pi Q}{r_+} {}_2F_1\left(\frac{1}{4}, \frac{1}{2}, \frac{5}{4}; -\frac{aQ^2}{r_+^4}\right), \quad (59)$$

where ${}_2F_1(a, b, c; x)$ is the hypergeometric function.

The equation of state (46) becomes

$$\tilde{T}(\tilde{r}_+) \equiv \frac{h(\tilde{r}_+)}{4\pi\tilde{r}_+} = \frac{1}{4\pi\tilde{r}_+} \left(1 + 3\tilde{r}_+^2 - \frac{1}{2} \frac{\tilde{Q}^2}{\tilde{r}_+^2 + \sqrt{\tilde{r}_+^4 + \tilde{a}\tilde{Q}^2}} \right), \quad (60)$$

where $\tilde{a} = a/l^2$, and we define $h(\tilde{r}_+)$ for later use. Noting that $h(0) = 1 - \frac{\tilde{Q}}{2\sqrt{\tilde{a}}}$, $h(\infty) \rightarrow +\infty$ and $h(\tilde{r}_+)$ is a strictly increasing function, one finds that

$$\begin{aligned} Q^2 \geq 4a: \quad & \tilde{T}(\tilde{r}_+) = 0 \text{ has only one solution } \tilde{r}_+ = \tilde{r}_e \geq 0, \\ Q^2 < 4a: \quad & \tilde{T}(\tilde{r}_+) > 0 \text{ for } \tilde{r}_+ \geq 0, \end{aligned}$$

where \tilde{r}_e corresponds to an extremal black hole.

To study behavior of local extremums of $\tilde{T}(\tilde{r}_+)$, we consider the equation $\tilde{T}''(\tilde{r}_+) = 0$, which becomes

$$z(x) \equiv x^3 - \frac{3\tilde{Q}^2}{2}x^2 + \tilde{a}\tilde{Q}^4 = 0, \quad (61)$$

with $x = \sqrt{\tilde{a}\tilde{Q}^2 + \tilde{r}_+^4}$. Since $\lim_{x \rightarrow \pm\infty} z(x) = \pm\infty$, $z'(0) = 0$ and $z'(\tilde{Q}^2) = 0$, $z(x)$ has a local maximum of $z(0) = \tilde{a}\tilde{Q}^4 > 0$ at $x = 0$ and a local minimum of $z(\tilde{Q}^2) = (-\tilde{Q}^2/2 + \tilde{a})\tilde{Q}^4$ at $x = \tilde{Q}^2$. If the local minimum is not greater than zero ($Q^2 \geq 2a$), there are two positive real roots $x_1 \geq \tilde{Q}^2 \geq x_2 > 0$ to the equation (61). Otherwise ($Q^2 < 2a$), this equation has no positive real roots. To make $\tilde{r}_+ = (x^2 - \tilde{a}\tilde{Q}^2)^{1/4}$ real, we also require $x \geq \sqrt{\tilde{a}\tilde{Q}}$. For x_1 , one always has that $x_1 \geq \tilde{Q}^2 > \sqrt{\tilde{a}\tilde{Q}}$ since $Q^2 \geq 2a$. To have $x_2 \geq \sqrt{\tilde{a}\tilde{Q}}$, we need to have $z(\sqrt{\tilde{a}\tilde{Q}}) \leq 0 \Rightarrow Q^2 \geq 4a$. With solutions of $\tilde{T}''(\tilde{r}_+) = 0$, it is easy to analyze the existence of the local extremums of $\tilde{T}(\tilde{r}_+)$, results of which are summarized in Table I.

	$\tilde{T}'(0)$	$\tilde{T}'(+\infty)$	Solution of $\tilde{T}''(\tilde{r}_+) = 0$	Extremums of $\tilde{T}(\tilde{r}_+)$
$Q^2 > 4a$	$+\infty$	$3/4\pi$	$\tilde{r}_1 > 0$	Minimum at $\tilde{r}_+ = \tilde{r}_1$
$Q^2 = 4a$	> 0	$3/4\pi$	$\tilde{r}_1 > 0, 0$	Minimum at $\tilde{r}_+ = \tilde{r}_1$
$4a > Q^2 > 2a$	$-\infty$	$3/4\pi$	$\tilde{r}_1 > \tilde{r}_2 > 0$	Minimum/Maximum at $\tilde{r}_+ = \tilde{r}_1/\tilde{r}_2$
$Q^2 = 2a$	$-\infty$	$3/4\pi$	$\tilde{r}_1 > 0, \tilde{T}''(\tilde{r}_+) \geq 0$	None
$Q^2 < 2a$	$-\infty$	$3/4\pi$	None, $\tilde{T}''(\tilde{r}_+) > 0$	None

TABLE I: Solution of $\tilde{T}''(\tilde{r}_+) = 0$ and the local extremums of $\tilde{T}(\tilde{r}_+)$ in various cases, where $\tilde{r}_i = (x_i^2 - \tilde{a}\tilde{Q}^2)^{1/4}$.

When solving eqn. (60) for \tilde{r}_+ in terms of \tilde{T} , the solution $\tilde{r}_+(\tilde{T})$ is often a multivalued function. The parameters \tilde{a} and \tilde{Q} determine the number of the branches of $\tilde{r}_+(\tilde{T})$ and the phase structure of the black hole. In what follows, we find six regions in the \tilde{a} - \tilde{Q} plane, in each of which the black hole has the distinct behavior of the branches and the phase structure:

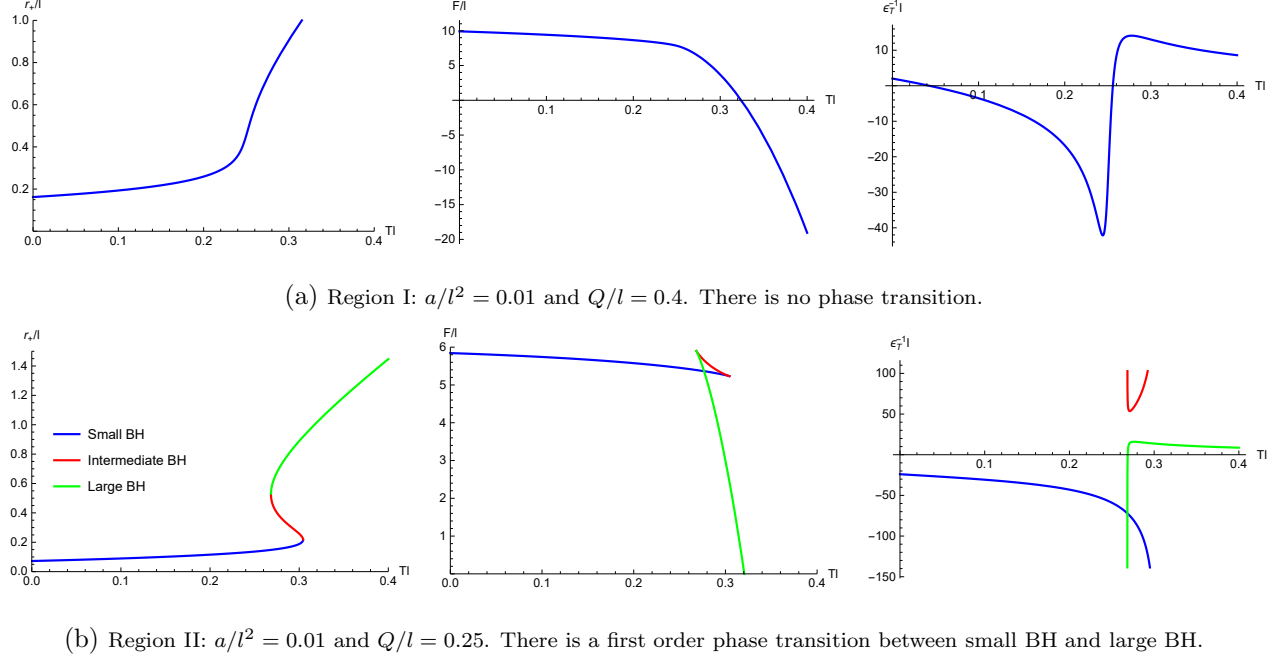
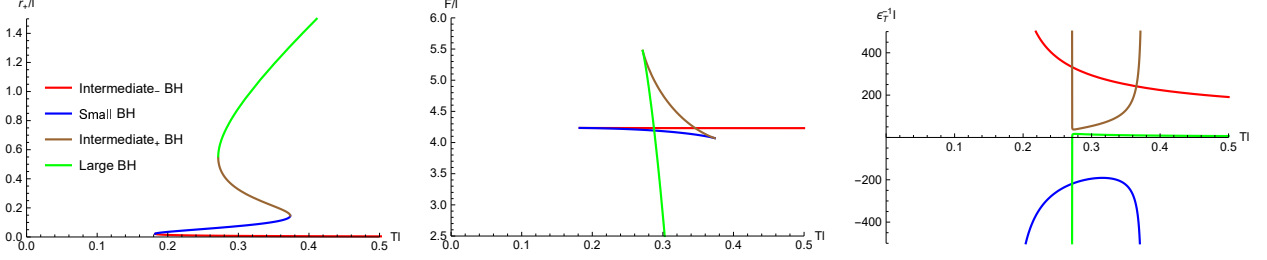
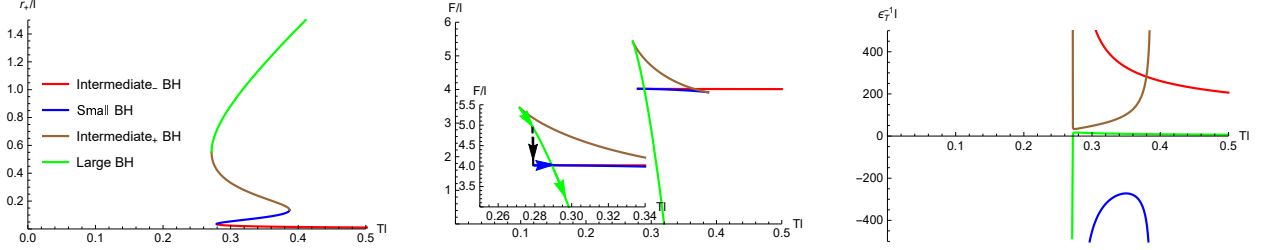


FIG. 2: Plot of \tilde{r}_+ , \tilde{F} and $\epsilon_T^{-1}l$ against \tilde{T} for BI-AdS black holes in Regions I and II. Black holes in these regions are RN type since there exist extremal black hole solutions. Regions I and II can be considered as reminiscent of RN-AdS black holes. The blue and green branches are thermally stable.

- Region I: $Q^2 \geq 4a$ and $\tilde{T}'(\tilde{r}_1) \geq 0$. In this region, $\tilde{T}'(\tilde{r}_+) \geq \tilde{T}'(\tilde{r}_1) \geq 0$ and hence $\tilde{T}(\tilde{r}_+)$ is an increasing function. So there is only one branch for $\tilde{r}_+(\tilde{T})$, which is thermally stable. Since $\tilde{T}(\tilde{r}_+) = 0$ has a solution in this region, this branch can extend to zero temperature. For a black hole with $\tilde{a} = 0.01$ and $\tilde{Q} = 0.4$ in this region, we plot the radius \tilde{r}_+ , the Gibbs energy \tilde{F} and the isothermal permittivity $\epsilon_T^{-1}l$ as functions of \tilde{T} in FIG. 2(a), which shows that this black hole is electrically stable for small enough and large enough \tilde{T} . However for large enough \tilde{a} , the black hole is always electrically stable.
- Region II: $Q^2 \geq 4a$ and $\tilde{T}'(\tilde{r}_1) < 0$. In this region, $\tilde{T}'(\tilde{r}_+) = 0$ has two solutions $\tilde{r}_+ = \tilde{r}_{\max}$ and \tilde{r}_{\min} with $\tilde{r}_{\max} < \tilde{r}_1 < \tilde{r}_{\min}$. Since $\tilde{T}(+\infty) = +\infty$, $\tilde{T}(\tilde{r}_+)$ has a local

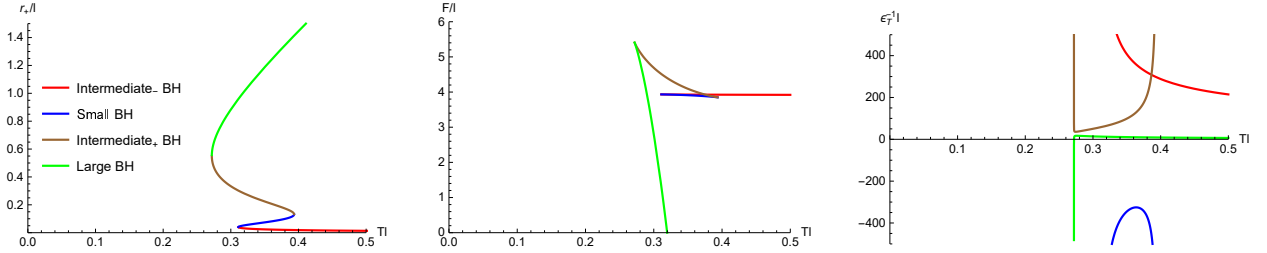


(a) Region III: $a/l^2 = 0.01$ and $Q/l = 0.195$. There is a first order phase transition between small BH and large BH.

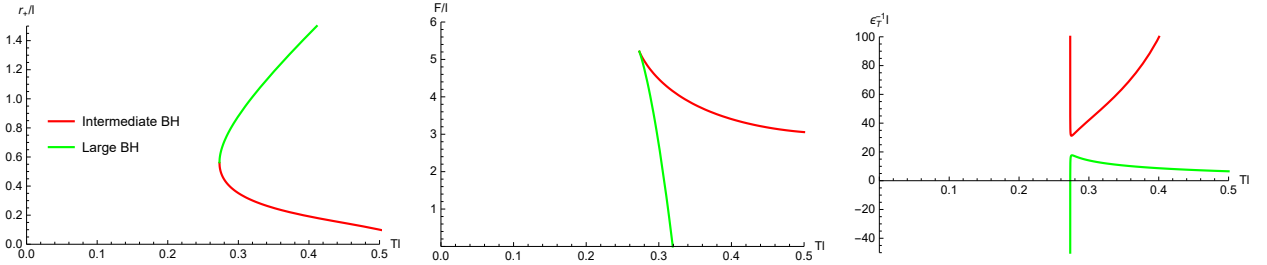


(b) Region IV: $a/l^2 = 0.01$ and $Q/l = 0.188$. The arrows in the inset indicate increasing \tilde{T} . As \tilde{T} increases, the black hole jumps from the large BH branch to the small BH one, corresponding to the zeroth order phase transition between small BH and large BH. Further increasing \tilde{T} , there would be a first order phase transition returning to large BH. Here we observe

LBH/SBH/LBH reentrant phase transition.



(c) Region V: $a/l^2 = 0.01$ and $Q/l = 0.185$. There is no phase transition.



(d) Region VI: $a/l^2 = 0.01$ and $Q/l = 0.15$. There is no phase transition.

FIG. 3: Plot of \tilde{r}_+ , \tilde{F} and $\epsilon_T^{-1}l$ against \tilde{T} for BI-AdS black holes in Regions III, IV, V and VI. Black holes in these regions are Schwarzschild-like type since they only exist for large enough \tilde{T} . The blue and green branches are always thermally stable. Small BH is electrically unstable while large BH is almost electrically stable.

maximum of $\tilde{T}_{\max} = \tilde{T}(\tilde{r}_{\max})$ at $\tilde{r}_+ = \tilde{r}_{\max}$ and a local minimum of $\tilde{T}_{\min} = \tilde{T}(\tilde{r}_{\min})$ at $\tilde{r}_+ = \tilde{r}_{\min}$. There are three branches for $\tilde{r}_+(\tilde{T})$: small BH for $0 \leq \tilde{T} \leq \tilde{T}_{\max}$, intermediate BH for $\tilde{T}_{\min} \leq \tilde{T} \leq \tilde{T}_{\max}$ and large BH for $\tilde{T} \geq \tilde{T}_{\min}$, which are displayed in the left panel of FIG. 2(b). The Gibbs free energy of the three branches is plotted in the middle panel, which shows that there is a first order phase transition between small BH and large BH occurring at $\tilde{T} = \tilde{T}_{\text{first}}$ with $\tilde{T}_{\min} \leq \tilde{T}_{\text{first}} \leq \tilde{T}_{\max}$. Both the small BH and large BH branches are thermally stable. As explained in section II, ϵ_T^{-1} of small BH goes to $-\infty$ as $\tilde{T} \rightarrow \tilde{T}_{\max}$ while that of large BH goes to $+\infty$ as $\tilde{T} \rightarrow \tilde{T}_{\min}$. The right panel shows that small BH is electrically unstable while large BH is almost electrically stable.

- Region III: $4a > Q^2 > 2a$, $\tilde{T}'(\tilde{r}_1) < 0$, $\tilde{T}'(\tilde{r}_2) > 0$ and $\tilde{T}(\tilde{r}_{\min 2}) < \tilde{T}(\tilde{r}_{\min 1})$. In this region, $\tilde{T}'(\tilde{r}_+) = 0$ has three solutions $\tilde{r}_+ = \tilde{r}_{\max}$, $\tilde{r}_{\min 1}$ and $\tilde{r}_{\min 2}$ with $\tilde{r}_{\min 2} < \tilde{r}_2 < \tilde{r}_{\max} < \tilde{r}_1 < \tilde{r}_{\min 1}$. So $\tilde{T}(\tilde{r}_+)$ has a local maximum of $\tilde{T}_{\max} = \tilde{T}(\tilde{r}_{\max})$ at $\tilde{r}_+ = \tilde{r}_{\max}$, a local minimum of $\tilde{T}_{\min 1} = \tilde{T}(\tilde{r}_{\min 1})$ at $\tilde{r}_+ = \tilde{r}_{\min 1}$ and a global minimum of $\tilde{T}_{\min 2} = \tilde{T}(\tilde{r}_{\min 2})$ at $\tilde{r}_+ = \tilde{r}_{\min 2}$. There are four branches for $\tilde{r}_+(\tilde{T})$: intermediate₋ BH for $\tilde{T} \geq \tilde{T}_{\min 2}$, small BH for $\tilde{T}_{\min 2} \leq \tilde{T} \leq \tilde{T}_{\max}$, intermediate₊ BH for $\tilde{T}_{\min 1} \leq \tilde{T} \leq \tilde{T}_{\max}$ and large BH for $\tilde{T} \geq \tilde{T}_{\min 1}$, which are displayed in the left panel of FIG. 3(a). Note that there is no black hole solution when $\tilde{T} < \tilde{T}_{\min 2}$. The Gibbs free energy of the four branches is plotted in the middle panel, which shows that there is a first order phase transition between small BH and large BH occurring at $\tilde{T} = \tilde{T}_{\text{first}}$ with $\tilde{T}_{\min 2} \leq \tilde{T}_{\text{first}} \leq \tilde{T}_{\max}$. Both the small BH and large BH branches are thermally stable, while intermediate_± BH branches are not. Similarly to Region II, the right panel shows that small BH is electrically unstable while large BH is almost electrically stable.
- Region IV: $4a > Q^2 > 2a$, $\tilde{T}'(\tilde{r}_1) < 0$, $\tilde{T}'(\tilde{r}_2) > 0$, $\tilde{T}_{\min 2} \geq \tilde{T}_{\min 1}$ and $\tilde{F}_S(\tilde{T}_{\min 2}) < \tilde{F}_L(\tilde{T}_{\min 2})$, where $\tilde{F}_{S/L}$ is the Gibbs free energy of the small/large BH branch. In this region, $\tilde{T}(\tilde{r}_+)$ has a local maximum of $\tilde{T}_{\max} = \tilde{T}(\tilde{r}_{\max})$ at $\tilde{r}_+ = \tilde{r}_{\max}$, a local minimum of $\tilde{T}_{\min 2} = \tilde{T}(\tilde{r}_{\min 2})$ at $\tilde{r}_+ = \tilde{r}_{\min 2}$ and a global minimum of $\tilde{T}_{\min 1} = \tilde{T}(\tilde{r}_{\min 1})$ at $\tilde{r}_+ = \tilde{r}_{\min 1}$. There are four branches for $\tilde{r}_+(\tilde{T})$: intermediate₋ BH for $\tilde{T} \geq \tilde{T}_{\min 2}$, small BH for $\tilde{T}_{\min 2} \leq \tilde{T} \leq \tilde{T}_{\max}$, intermediate₊ BH for $\tilde{T}_{\min 1} \leq \tilde{T} \leq \tilde{T}_{\max}$ and large BH for $\tilde{T} \geq \tilde{T}_{\min 1}$, which are displayed in the left panel of FIG. 3(b). The Gibbs free energy of the four branches is plotted in the middle panel. As \tilde{T} increases from $\tilde{T}_{\min 1}$,

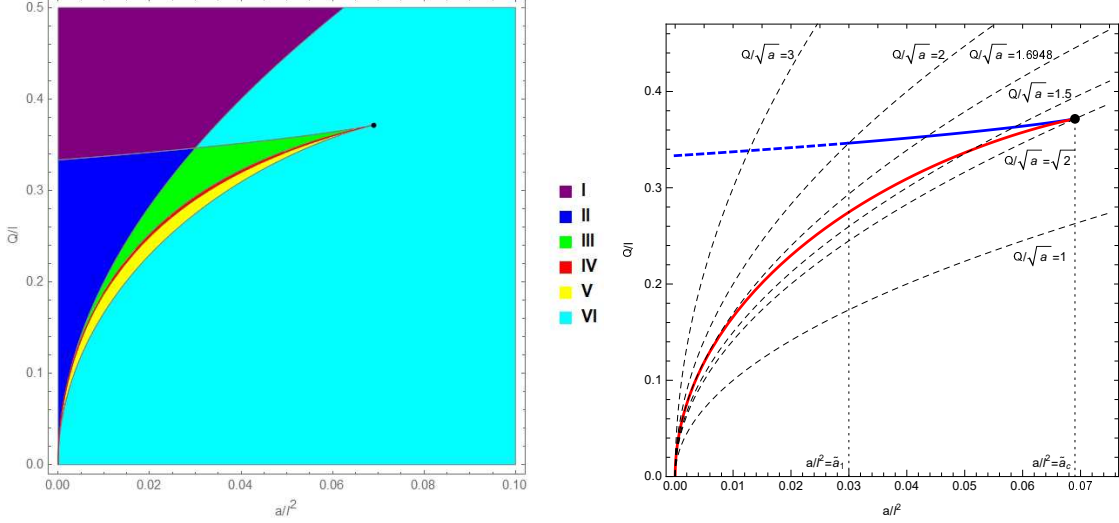
the black hole follows direction of arrows in the inset. It shows that there is a finite jump in Gibbs free energy leading to a zeroth order phase transition from large BH to small BH, followed by a first order phase transition returning to large BH. This LBH/SBH/LBH transition corresponds to a reentrant phase transition.

- Region V: $4a > Q^2 > 2a$, $\tilde{T}'(\tilde{r}_1) < 0$, $\tilde{T}'(\tilde{r}_2) > 0$, $\tilde{T}_{\min 2} > \tilde{T}_{\min 1}$ and $\tilde{F}_S(\tilde{T}_{\min 2}) \geq \tilde{F}_L(\tilde{T}_{\min 2})$. As shown in the left panel of FIG. 3(c), the four branches of $\tilde{r}_+(\tilde{T})$ in this region are the same as in Region IV. However, the middle panel shows that the large BH branch is always thermodynamically preferred for $\tilde{T} \geq \tilde{T}_{\min 1}$, and hence there is no phase transition in this region.
- Region VI: $4a > Q^2 > 2a$ and $\tilde{T}'(\tilde{r}_1) > 0$ or $\tilde{T}'(\tilde{r}_2) < 0$; or $Q^2 < 2a$. It can show that $\tilde{T}'(\tilde{r}_+) = 0$ has only one solution $\tilde{r}_+ = \tilde{r}_{\min}$ in this region. Since $\tilde{T}(+\infty) = +\infty$, $\tilde{T}(\tilde{r}_+)$ has a global minimum of $\tilde{T}_{\min} = \tilde{T}(\tilde{r}_{\min})$ at $\tilde{r}_+ = \tilde{r}_{\min}$. As shown in the left panel of FIG. 3(d), there are two branches for $\tilde{r}_+(\tilde{T})$: large BH and intermediate BH for $\tilde{T} \geq \tilde{T}_{\min}$. The middle panel shows that the large BH branch is always thermodynamically preferred for $\tilde{T} \geq \tilde{T}_{\min}$, and hence there is no phase transition in this region. This region is similar to the Schwarzschild-AdS case. The large BH branch is thermally stable and almost electrically stable.

In FIG. 4(a), we plot these six regions in the \tilde{a} - \tilde{Q} plane. It is interesting to note that the boundary between the region in which $\tilde{T}(\tilde{r}_+)$ has n extremums and that in which $\tilde{T}(\tilde{r}_+)$ has $n + 2$ extremums is the critical line, determined by

$$\frac{\partial \tilde{T}(\tilde{r}_+, \tilde{Q}, \tilde{a})}{\partial \tilde{r}_+} = 0 \text{ and } \frac{\partial^2 \tilde{T}(\tilde{r}_+, \tilde{Q}, \tilde{a})}{\partial \tilde{r}_+^2} = 0. \quad (62)$$

There are 3 such boundaries in FIG. 4(a), i.e., $\tilde{Q}_{12}(\tilde{a})$, $\tilde{Q}_{36}(\tilde{a})$, $\tilde{Q}_{56}(\tilde{a})$, where $\tilde{Q}_{ij}(\tilde{a})$ is the boundary Region i and Region j . As shown in FIG. 4(a), the critical line has two branches: $\tilde{Q}_{c1}(\tilde{a}) = \{\tilde{Q}_{12}(\tilde{a}), \tilde{Q}_{36}(\tilde{a})\}$ and $\tilde{Q}_{c2}(\tilde{a}) = \tilde{Q}_{56}(\tilde{a})$. We plot these two branches of the critical line in FIG. 4(b), where $\tilde{Q}_{c1}(\tilde{a})$ is the blue line, and $\tilde{Q}_{c2}(\tilde{a})$ is the red line. Note that $\tilde{Q}_{c1}(\tilde{a})$ and $\tilde{Q}_{c2}(\tilde{a})$ meet and terminate at $\{\tilde{a}_c, \tilde{Q}_c\} \simeq \{0.069, 0.37\}$, which is represented by the black point in FIG. 4. However, the middle panel of FIG. 3(c) shows that the branch $\tilde{Q}_{c2}(\tilde{a})$ is not physical since it does not globally minimize the Gibbs free energy. So the critical line has only one physical branch, $\tilde{Q}_{c1}(\tilde{a})$, which is marked by the blue line. For



(a) The six regions in the \tilde{a} - \tilde{Q} plane, each of which possesses the distinct behavior of the branches and the phase structure for BI-AdS black holes. The LBH/SBH/LBH reentrant phase transition occurs in Region IV. The LBH/SBH first order phase transition occurs in Regions II and III. No phase transitions occur in Regions I, V and VI.

(b) The critical line has two branches, and the physical/unphysical one is depicted by the blue/red line. $\tilde{Q}_l(\tilde{a})$ is plotted for various values of $Q/\sqrt{\tilde{a}}$. There is no critical point for $Q/\sqrt{\tilde{a}} < \sqrt{2}$, while there exists one physical critical point for $Q/\sqrt{\tilde{a}} > \sqrt{2}$. The black hole also possesses an unphysical critical point for $\sqrt{2} < Q/\sqrt{\tilde{a}} < 1.6948$.

FIG. 4: The six regions and the critical line in the \tilde{a} - \tilde{Q} plane for BI-AdS black holes. The critical line consists of $\tilde{Q}_{12}(\tilde{a})$ (the blue dashed line), $\tilde{Q}_{36}(\tilde{a})$ (the blue solid line) and $\tilde{Q}_{56}(\tilde{a})$ (the red line), where $\tilde{Q}_{ij}(\tilde{a})$ is the boundary Region i and Region j . With fixed Q and a , the black hole moves along the curve $\tilde{Q}_l(\tilde{a}) = \frac{Q}{\sqrt{\tilde{a}}}\sqrt{\tilde{a}}$ by varying P .

$\tilde{a} \leq \tilde{a}_1 \simeq 0.030$, $\tilde{Q}_{c1}(\tilde{a})$ is $\tilde{Q}_{12}(\tilde{a})$ and depicted by the blue dashed line in FIG. 4(b). This part of $\tilde{Q}_{c1}(\tilde{a})$ is reminiscent of RN-AdS black holes.

We now discuss the critical behavior and phase structure of black holes in two cases. In the first case, Q and a are fixed parameters, and the AdS radius l (the pressure P) varies. With fixed values of Q and a , varying l would generate a curve in the \tilde{a} - \tilde{Q} plane, which is determined by

$$\tilde{Q}_l(\tilde{a}) = \frac{Q}{\sqrt{\tilde{a}}}\sqrt{\tilde{a}}. \quad (63)$$

In FIG. 4(b), we plot $\tilde{Q}_l(\tilde{a})$ for various values of $Q/\sqrt{\tilde{a}}$. It shows that, for $Q/\sqrt{\tilde{a}} < \sqrt{2}$,

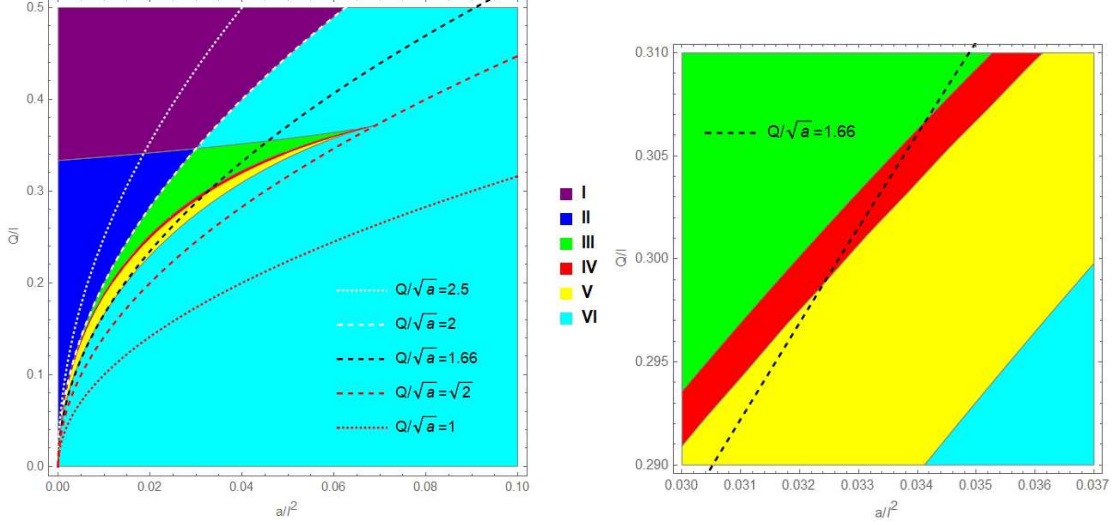


FIG. 5: In the case of varying P with fixed Q and a , the system moves along $\tilde{Q}_l(\tilde{a})$, which is displayed for various values of Q/\sqrt{a} . For $Q/\sqrt{a} < \sqrt{2}$, there is no phase transition in the system. For $Q/\sqrt{a} > \sqrt{2}$, there is one critical point and the corresponding LBH/SBH first order phase transition. In addition, for $\sqrt{2} < Q/\sqrt{a} < 2$, there is a LBH/SBH zeroth order phase transition occurring in Region IV, corresponding to the LBH/SBH/LBH reentrant phase transition.

there is no critical point for black holes. For $Q/\sqrt{a} > \sqrt{2}$, there exists one physical critical point. Moreover, the critical behavior is reminiscent of RN-AdS black holes for $Q/\sqrt{a} > 2$. Note that $\tilde{Q}_l(\tilde{a})$ intersects the unphysical branch $\tilde{Q}_{c2}(\tilde{a})$ for $1.6948 > Q/\sqrt{a} > \sqrt{2}$. The phase structure of $\tilde{Q}_l(\tilde{a})$ can be read from FIG. 5. It shows that for $Q/\sqrt{a} < 2$, $\tilde{Q}_l(\tilde{a})$ is always in Region VI, and hence there is no first order phase transition. For $Q/\sqrt{a} > 2$, as one starts from $P = 0$, $\tilde{Q}_l(\tilde{a})$ is in Region II, in which there is a first order phase transition between small BH and large BH. Further increasing P , $\tilde{Q}_l(\tilde{a})$ goes through the critical line and enters the Region I, in which there is no phase transition. This behavior is reminiscent of that of the RN-AdS black hole. For $\sqrt{2} < Q/\sqrt{a} < 2$, as P increases from $P = 0$, $\tilde{Q}_l(\tilde{a})$ starts from Region VI, crosses the unphysical critical line and enters Region V, during which no phase transition occurs. Further increasing P , $\tilde{Q}_l(\tilde{a})$ enters Region IV, in which there is a reentrant phase transition occurring for some range of P . As P continuously increases, $\tilde{Q}_l(\tilde{a})$ enters Region III, in which a first order phase transition occurs, crosses the critical line and returns to Region V. The critical behavior and phase structure in this case has been

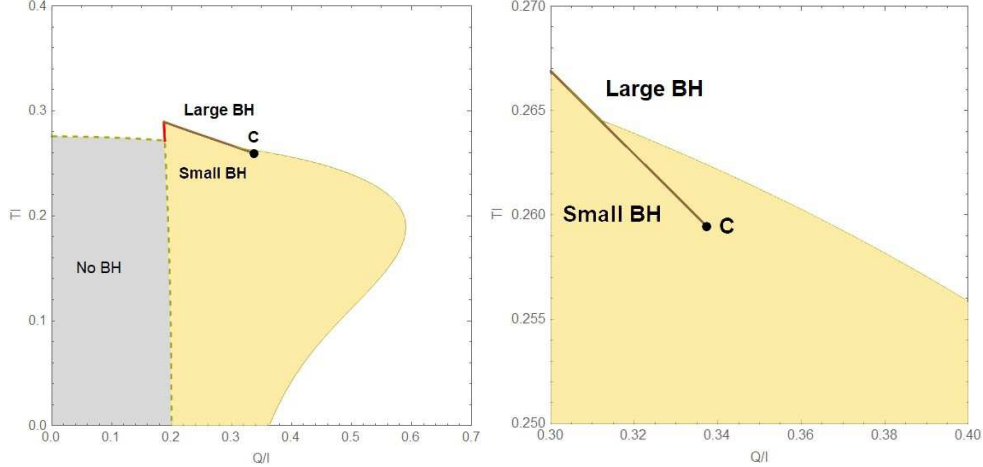


FIG. 6: The phase diagram in the \tilde{Q} - \tilde{T} plane for BI-AdS black holes with $a/l^2 = 0.01$. The first order phase transition line separating large BH and small BH is displayed by the brown line, and it terminates at the critical point, marked by the black dot. There is also a zeroth order phase transition line, depicted by the red line. All phases in the diagram are thermally stable. However, the phases in the yellow region are electrically unstable. Large BH above the first order phase transition line is always electrically stable except in the region around the critical point, which are highlighted in the right panel. It shows that the critical point is in the yellow region.

discussed in [19]^[1], which are correctly reproduced here.

In the second case, a and $P(l)$ are fixed parameters, and one varies Q . FIGs. 4 show that for $a/l^2 > \tilde{a}_c$, there is no critical point, and no phase transition occurs. For $a/l^2 < \tilde{a}_c$, there is one critical point. As one increases Q from $Q = 0$, the black hole would experience different regions, in which there occur no phase transition \rightarrow the LBH/SBH/LBH reentrant phase transition \rightarrow the LBH/SBH first order phase transition \rightarrow no phase transition. For $a/l^2 < \tilde{a}_1$ and large enough values of Q , the black hole is in Regions I and II, in which the phase transition behavior is reminiscent of the RN-AdS black hole. The critical behavior and phase structure in this case has also been studied in [48].

The phase diagram of the BI-AdS black hole for $a/l^2 = 0.01$ is displayed in the \tilde{Q} - \tilde{T} plane in FIG. 6. There is a LBH/SBH first order transition for some range of \tilde{Q} and a LBH/SBH zeroth order phase transition for some smaller range of \tilde{Q} . The zeroth and first

[1] In [19], their b is our $\frac{1}{4\sqrt{a}}$.

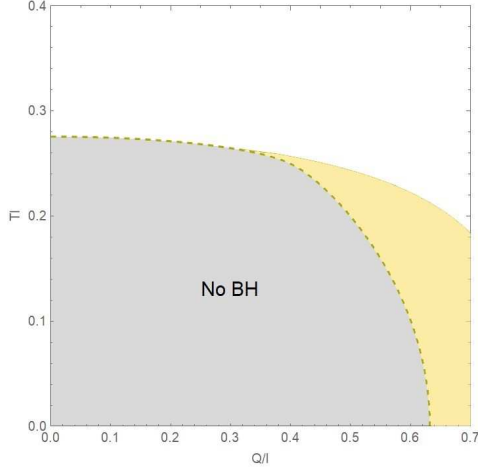


FIG. 7: The phase diagram in the \tilde{Q} - \tilde{T} plane for BI-AdS black holes with $a/l^2 = 0.1$. There are no phase transitions. The black holes in the yellow region are electrically unstable..

order phase transitions are marked by the red and brown lines, respectively. The first order phase transition line terminates at the critical point, represented by the black point. No BH region means that no black hole solutions exist. As discussed before, the black hole solutions in the phase diagram are thermally stable. However, the solutions in the yellow region are unstable to electrical fluctuations. Small BH below the first order phase transition line is always electrically unstable while large BH above the line is almost electrically stable. The right panel of FIG. 6 shows that large BH is only electrically unstable in the region around the critical point. Note that the black hole solution at the critical point is electrically unstable.

The phase diagram of the BI-AdS black hole for $a/l^2 = 0.1$ is displayed in the \tilde{Q} - \tilde{T} plane in FIG. 7, which is simpler than that for $a/l^2 = 0.01$. FIG. 4 shows that when $a/l^2 > \tilde{a}_c \simeq 0.069$ (the black dot), black holes are Regions I or VI, in which no phase transition occurs. At low temperatures, the black hole solution is electrically unstable for small enough values of Q/l .

IV. IBORN-INFELD ADS BLACK HOLE

We now consider an iBorn-Infeld field with the Lagrangian density

$$\mathcal{L}(s) = -\frac{1}{a} \left(1 - \sqrt{1 + 2as} \right), \quad (64)$$

where $a > 0$. For an iBorn-Infeld AdS (iBI-AdS) black hole solution, $f(r)$ in the black hole solution (7) is given by

$$f(r) = 1 - \frac{M}{8\pi r} + \frac{r^2}{l^2} - \frac{Q^2}{6\sqrt{r^4 - aQ^2} + 6r^2} + \frac{Q^2}{3r^2} {}_2F_1\left(\frac{1}{4}, \frac{1}{2}, \frac{5}{4}; \frac{aQ^2}{r^4}\right), \quad (65)$$

where M and Q are the mass and the charge of the black hole, respectively. For $A'_t(r)$, one has

$$A'_t(r) = \frac{Q}{\sqrt{r^4 - aQ^2}}, \quad (66)$$

which gives the potential of the black hole

$$\Phi = \frac{4\pi Q}{r_+} {}_2F_1\left(\frac{1}{4}, \frac{1}{2}, \frac{5}{4}; \frac{aQ^2}{r_+^4}\right). \quad (67)$$

This iBI-AdS black hole solution has a singularity at $r = r_s$, where we define

$$r_s \equiv a^{1/4}Q^{1/2}. \quad (68)$$

To study the nature of this singularity, we compute the corresponding Ricci scalar:

$$R = \frac{2}{a} - 12 + \frac{1}{ar^2} \frac{r^4 - 2r^4}{\sqrt{r^4 - r_s^4}}, \quad (69)$$

which becomes divergent at $r = r_s$. So the singularity at $r = r_s$ is a physical singularity, and one requires that $r > r_s$.

The equation of state (46) becomes

$$\tilde{T}(\tilde{r}_+) \equiv \frac{h(\tilde{r}_+)}{4\pi\tilde{r}_+} = \frac{1}{4\pi\tilde{r}_+} \left(1 + 3\tilde{r}_+^2 - \frac{1}{2} \frac{\tilde{Q}^2}{\tilde{r}_+^2 + \sqrt{\tilde{r}_+^4 - \tilde{a}\tilde{Q}^2}} \right),$$

where $\tilde{r}_+ > \tilde{r}_s \equiv \tilde{a}^{1/4}\tilde{Q}^{1/2}$, $\tilde{a} = a/l^2$ and $\tilde{Q} = Q/l$. It can show that $h(\tilde{r}_+)$ is a strictly increasing function and $h(\infty) \rightarrow +\infty$. At $\tilde{r}_+ = \tilde{r}_s$, one has

$$h(\tilde{r}_s) = 1 + 3\tilde{a}^{1/2}\tilde{Q} - \frac{\tilde{Q}}{2\tilde{a}^{1/2}}. \quad (70)$$

For $h(\tilde{r}_s) \leq 0$, which reduces to

$$\tilde{a} < \frac{1}{6} \text{ and } \tilde{Q} \geq \frac{2\sqrt{\tilde{a}}}{1 - 6\tilde{a}}, \quad (71)$$

$\tilde{T}(\tilde{r}_+) = 0$ has one solution $\tilde{r}_+ = \tilde{r}_e$, at which the black hole becomes extremal. In this case, the black hole is RN type. For $h(\tilde{r}_s) > 0$, which reduces to

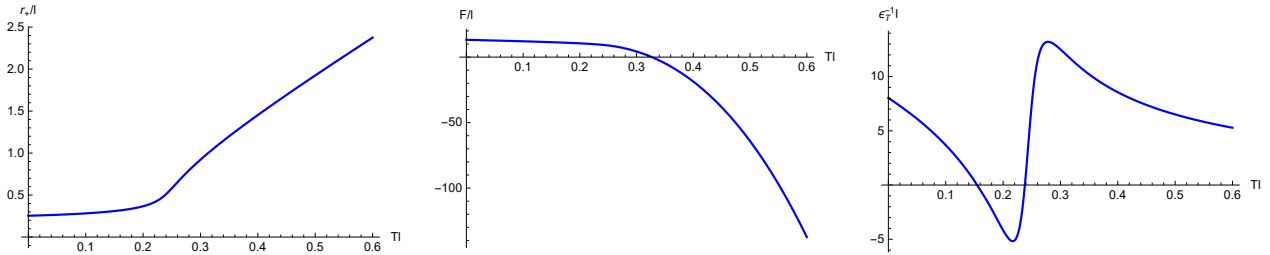
$$\tilde{a} < \frac{1}{6} \text{ and } \tilde{Q} < \frac{2\sqrt{\tilde{a}}}{1 - 6\tilde{a}}; \text{ or } \tilde{a} \geq \frac{1}{6}, \quad (72)$$

the temperature of the black hole has a positive minimum value, and the black hole is Schwarzschild-like type.

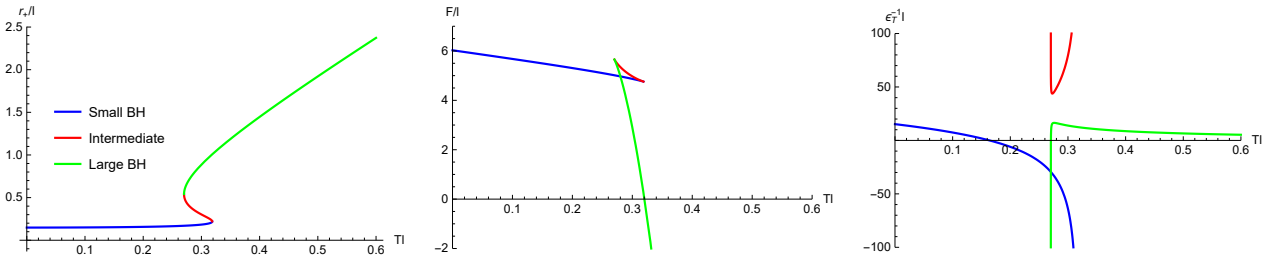
The equation $\tilde{T}''(\tilde{r}_+) = 0$ becomes

$$z(x) \equiv x^3 - \frac{3\tilde{Q}^2}{2}x^2 - \tilde{a}\tilde{Q}^4 = 0, \quad (73)$$

where $x = \sqrt{\tilde{r}_+^4 - \tilde{a}\tilde{Q}^2} > 0$. It can show that $z(x)$ has a local maximum of $z(0) = -\tilde{a}\tilde{Q}^4 < 0$ at $x = 0$ and a local minimum of $z(\tilde{Q}^2) = (-\tilde{Q}^2/2 - \tilde{a})\tilde{Q}^4 < 0$ at $x = \tilde{Q}^2$. So $z(x) = 0$ always admits one single positive real root $x = x_1 > 0$. Since $\lim_{\tilde{r}_+ \rightarrow \tilde{r}_s} \tilde{T}'(\tilde{r}_+) = +\infty$ and $\lim_{\tilde{r}_+ \rightarrow +\infty} \tilde{T}'(\tilde{r}_+) = 3\sqrt{\tilde{a}\tilde{Q}}$, $\tilde{T}'(\tilde{r}_+)$ always has a global minimum of $\tilde{T}'_{\min} \equiv \tilde{T}'(\tilde{r}_1)$ at $\tilde{r}_+ = \tilde{r}_1 \equiv (x_1^2 + \tilde{a}\tilde{Q}^2)^{1/4}$. In what follows, we also find six regions in the \tilde{a} - \tilde{Q} plane for iBI-AdS black holes, in each of which the black hole has the distinct behavior of the branches and the phase structure:



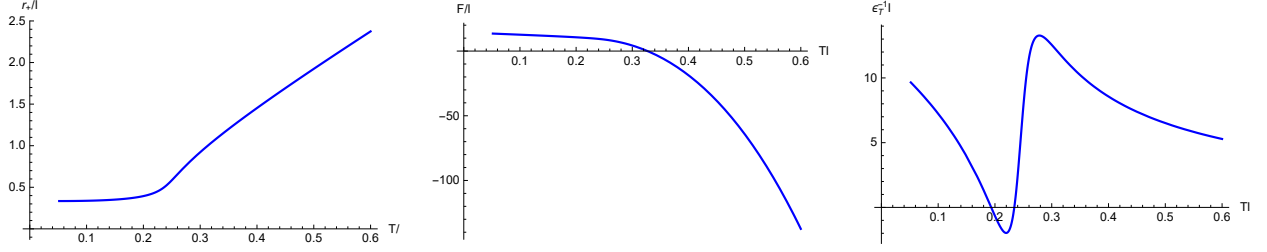
(a) Region I: $a/l^2 = 0.01$ and $Q/l = 0.5$. There is no phase transition.



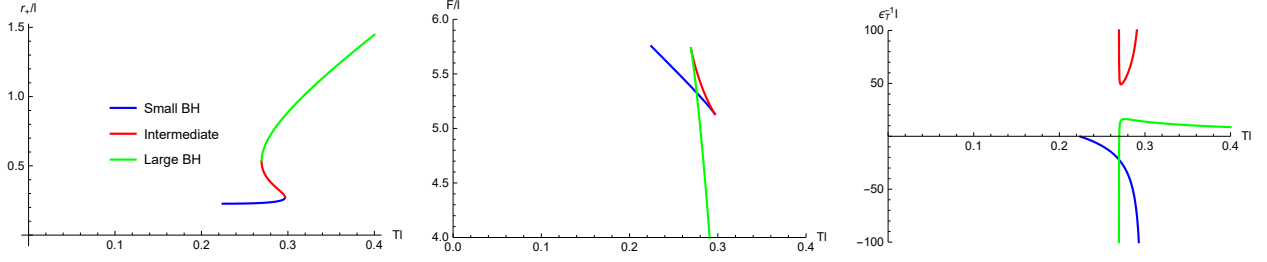
(b) Region II: $a/l^2 = 0.01$ and $Q/l = 0.22$. There is a first order phase transition between small BH and large BH.

FIG. 8: Plot of \tilde{r}_+ , \tilde{F} and $\epsilon_T^{-1}l$ against \tilde{T} for iBI-AdS black holes in Regions I and II, where Black holes in these regions are RN type. Regions I and II can be considered as reminiscent of RN-AdS black holes. The blue and green branches are thermally stable. It shows that for small enough \tilde{a} , e.g., $\tilde{a} = 0.01$, the small BH branch is electrically stable for $\tilde{T} < \tilde{T}_1$ and unstable for $\tilde{T} > \tilde{T}_1$ with some $\tilde{T}_1 > 0$.

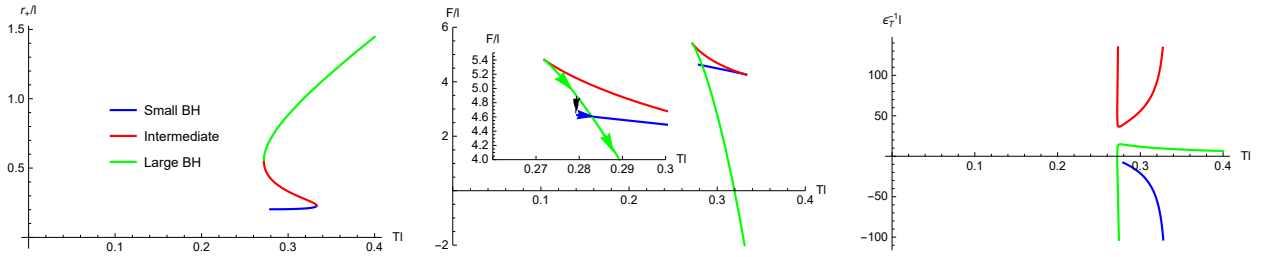
- Region I: $h(\tilde{r}_s) \leq 0$ and $\tilde{T}'_{\min} \geq 0$. Since $\tilde{T}'(\tilde{r}_+) \geq \tilde{T}'_{\min} \geq 0$, $\tilde{T}(\tilde{r}_+)$ is an increasing function in this region. So there is only one thermally stable branch for $\tilde{r}_+(\tilde{T})$. We plot



(a) Region III: $a/l^2 = 0.05$ and $Q/l = 0.5$. There is no phase transition.

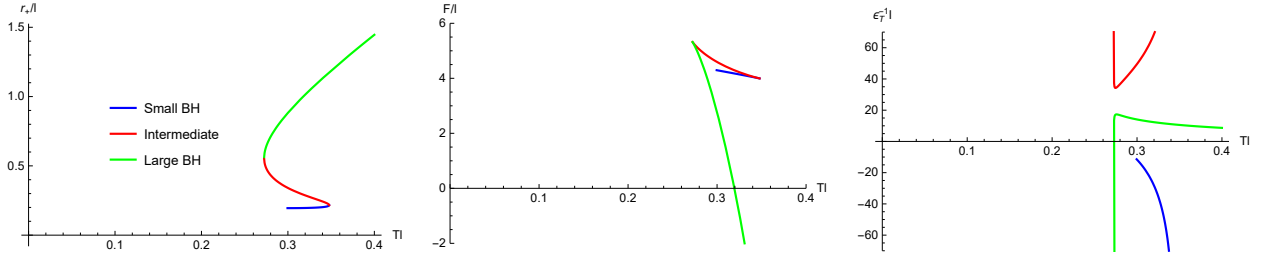


(b) Region IV: $a/l^2 = 0.05$ and $Q/l = 0.23$. There is a first order phase transition between small BH and large BH.



(c) Region V: $a/l^2 = 0.05$ and $Q/l = 0.184$. The arrows in the inset indicate increasing \tilde{T} . As \tilde{T} increases, the black hole jumps from the large BH branch to the small BH one, corresponding to the zeroth order phase transition between small BH and large BH. Further increasing \tilde{T} , there would be a first order phase transition returning to large BH. Here we observe

LBH/SBH/LBH reentrant phase transition.



(d) Region VI: $a/l^2 = 0.05$ and $Q/l = 0.17$. There is no phase transition.

FIG. 9: Plot of \tilde{r}_+ , \tilde{F} and $\epsilon_T^{-1}l$ against \tilde{T} for iBI-AdS black holes in Regions III, IV, V and VI. The temperature of black holes in these regions has a minimum value greater than zero. The blue and green branches are always thermally stable. It shows that for large enough \tilde{a} , e.g., $\tilde{a} = 0.05$, the small BH branch is always electrically unstable.

the radius \tilde{r}_+ , the Gibbs energy \tilde{F} and the isothermal permittivity $\epsilon_T^{-1}l$ as functions of \tilde{T} in FIG. 8(a) for a black hole with $\tilde{a} = 0.01$ and $\tilde{Q} = 0.5$ in this region. Moreover, this black hole is electrically stable for small enough and large enough values of \tilde{T} . However for large enough \tilde{a} , the black hole is always electrically stable.

- Region II: $h(\tilde{r}_s) \leq 0$ and $\tilde{T}'_{\min} < 0$. In this region, $\tilde{T}'(\tilde{r}_+) = 0$ has two solutions $\tilde{r}_+ = \tilde{r}_{\max}$ and \tilde{r}_{\min} with $\tilde{r}_{\max} < \tilde{r}_1 < \tilde{r}_{\min}$. Since $\tilde{T}(+\infty) = +\infty$, $\tilde{T}(\tilde{r}_+)$ has a local maximum of $\tilde{T}_{\max} \equiv \tilde{T}(\tilde{r}_{\max})$ at $\tilde{r}_+ = \tilde{r}_{\max}$ and a local minimum of $\tilde{T}_{\min} \equiv \tilde{T}(\tilde{r}_{\min})$ at $\tilde{r}_+ = \tilde{r}_{\min}$. There are three branches for $\tilde{r}_+(\tilde{T})$: small BH for $0 \leq \tilde{T} \leq \tilde{T}_{\max}$, intermediate BH for $\tilde{T}_{\min} \leq \tilde{T} \leq \tilde{T}_{\max}$ and large BH for $\tilde{T} \geq \tilde{T}_{\min}$, which are displayed in the left panel of FIG. 8(b). The middle panel shows that there is a first order phase transition between small BH and large BH occurring at $\tilde{T}_{\min} \leq \tilde{T} \leq \tilde{T}_{\max}$. Both the small BH and large BH branches are thermally stable. The right panel shows that large BH is almost electrically stable. However, the electrical stability of small BH depends on the values of \tilde{a} . For small enough \tilde{a} , e.g., $\tilde{a} = 0.01$, small BH is electrically stable for small enough \tilde{T} . For large enough \tilde{a} , small BH is always electrically unstable.
- Region III: $h(\tilde{r}_s) > 0$ and $\tilde{T}'_{\min} \geq 0$. As shown in FIG. 9(a), the black hole's temperature has a minimum of $\frac{h(\tilde{r}_s)}{4\pi r_s}$ at $\tilde{r}_+ = \tilde{r}_s$. There is only one branch for $\tilde{r}_+(\tilde{T})$ in this region, which is thermally stable. Similarly to Region I, the black hole is electrically unstable for some finite range of \tilde{T} for small enough \tilde{a} . However for large enough \tilde{a} , the black hole is always electrically stable.
- Region IV: $h(\tilde{r}_s) > 0$, $\tilde{T}'_{\min} < 0$ and $\tilde{T}_{\min} > \tilde{T}(\tilde{r}_s)$. In this region, $\tilde{T}'(\tilde{r}_+) = 0$ has two solutions $\tilde{r}_+ = \tilde{r}_{\max}$ and $\tilde{r}_+ = \tilde{r}_{\min}$ with $\tilde{r}_s < \tilde{r}_{\max} < \tilde{r}_1 < \tilde{r}_{\min}$. So $\tilde{T}(\tilde{r}_+)$ has a local maximum of \tilde{T}_{\max} at $\tilde{r}_+ = \tilde{r}_{\max}$, a local minimum of \tilde{T}_{\min} at $\tilde{r}_+ = \tilde{r}_{\min}$ and a global minimum of $\tilde{T}(\tilde{r}_s)$ at $\tilde{r}_+ = \tilde{r}_s$. There are three branches for $\tilde{r}_+(\tilde{T})$: small BH for $\tilde{T}(\tilde{r}_s) \leq \tilde{T} \leq \tilde{T}_{\max}$, intermediate BH for $\tilde{T}_{\min} \leq \tilde{T} \leq \tilde{T}_{\max}$ and large BH for $\tilde{T} \geq \tilde{T}_{\min}$, which are displayed in the left panel of FIG. 9(b). There is a first order phase transition between small BH and large BH occurring at $\tilde{T}_{\min} \leq \tilde{T} \leq \tilde{T}_{\max}$. Both the small BH and large BH branches are thermally stable, while the intermediate BH branch is not. The electrical stability of black holes in this region is similar to that in Region II.

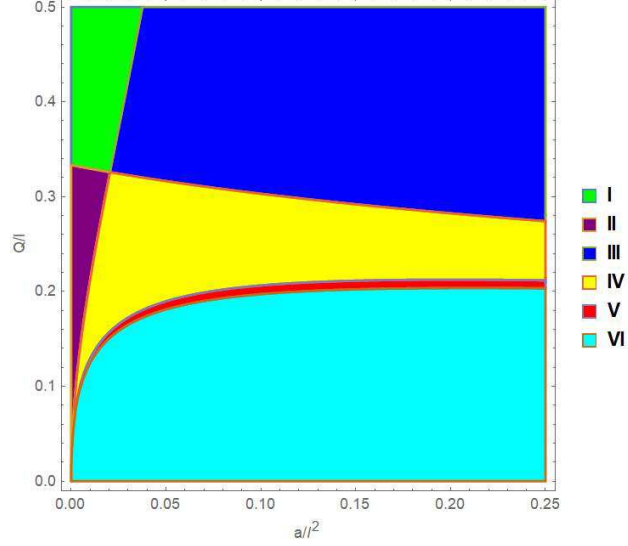
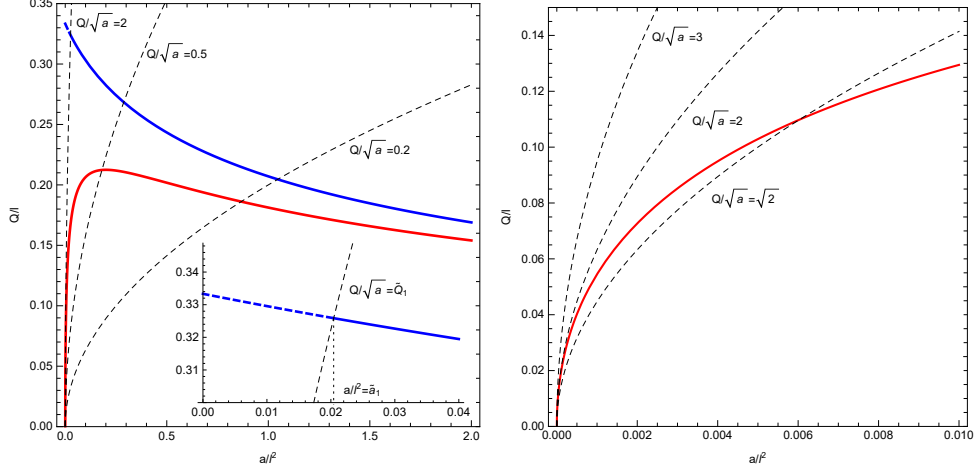


FIG. 10: The six regions in the \tilde{a} - \tilde{Q} plane, each of which possesses the distinct behavior of the branches and the phase structure for iBI-AdS black holes. The LBH/SBH/LBH reentrant phase transition occurs in Region V. The LBH/SBH first order phase transition occurs in Regions II and IV. No phase transitions occur in Regions I,III and VI.

- Region V: $h(\tilde{r}_s) > 0$, $\tilde{T}'_{\min} < 0$, $\tilde{T}_{\min} \leq \tilde{T}(\tilde{r}_s)$ and $\tilde{F}_S(\tilde{r}_s) < \tilde{F}_L(\tilde{r}_s)$, where $\tilde{F}_{S/L}$ is the Gibbs free energy of the small/large BH branch. In this region, $\tilde{T}(\tilde{r}_+)$ has a local maximum of \tilde{T}_{\max} at $\tilde{r}_+ = \tilde{r}_{\max}$, a global minimum of \tilde{T}_{\min} at $\tilde{r}_+ = \tilde{r}_{\min}$ and a local minimum of $\tilde{T}(\tilde{r}_s)$ at $\tilde{r}_+ = \tilde{r}_s$. FIG. 9(c) shows that there are three branches of $\tilde{r}_+(\tilde{T})$ in this region. The Gibbs free energy of the three branches is plotted in the middle panel. As \tilde{T} increases from \tilde{T}_{\min} , the black hole follows direction of arrows in the inset. It shows that at $\tilde{T} = \tilde{T}(\tilde{r}_s)$, there is a finite jump in Gibbs free energy leading to a zeroth order phase transition from large BH to small BH. Further increasing \tilde{T} , a first order phase transition returning to large BH occurs at $\tilde{T}(\tilde{r}_s) \leq \tilde{T} \leq \tilde{T}_{\max}$. This LBH/SBH/LBH transition corresponds to a reentrant phase transition.
- Region VI: $h(\tilde{r}_s) > 0$, $\tilde{T}'_{\min} < 0$, $\tilde{T}_{\min} \leq \tilde{T}(\tilde{r}_s)$ and $\tilde{F}_S(\tilde{r}_s) \geq \tilde{F}_L(\tilde{r}_s)$, As shown in the left panel of FIG. 9(d), there are three branches of $\tilde{r}_+(\tilde{T})$ in this region. The middle panel shows that the large BH branch is always thermodynamically preferred for $\tilde{T} \geq \tilde{T}_{\min}$, and hence there is no phase transition in this region.

These six regions are plotted in the \tilde{a} - \tilde{Q} plane in FIG. 10, from which the critical line



(a) There is always one physical critical point for the black holes on $\tilde{Q}_l(\tilde{a})$. For $Q/\sqrt{a} > \tilde{Q}_1 \simeq 2.28$, the inset displays that the critical point occurs for the Schwarzschild-like type black hole.

(b) For $Q/\sqrt{a} < 2$, $\tilde{Q}_l(\tilde{a})$ always intersect with $\tilde{Q}_{45}(\tilde{a})$. In this case, the black holes on $\tilde{Q}_l(\tilde{a})$ could be in Region V for some range of P , where the reentrant phase transition occurs.

FIG. 11: The blue line is the critical line, which consists of the boundaries $\tilde{Q}_{12}(\tilde{a})$ (the blue dashed line) and $\tilde{Q}_{34}(\tilde{a})$ (the blue solid line). The black hole on $\tilde{Q}_{12}(\tilde{a})$ is RN type. The red line is the boundary $\tilde{Q}_{45}(\tilde{a})$. In the case of varying P with fixed values of Q and a , the system moves along $\tilde{Q}_l(\tilde{a})$, which is plotted for various values of Q/\sqrt{a} .

can be read. In fact, the critical line is determined by $\tilde{T}'(\tilde{r}_1) = 0$ and hence is composed of $\tilde{Q}_{12}(\tilde{a})$ and $\tilde{Q}_{34}(\tilde{a})$, where $\tilde{Q}_{ij}(\tilde{a})$ is the boundary between Region i and Region j . The critical line is plotted in FIG. 11(a), and $\tilde{Q}_{12}(\tilde{a})/\tilde{Q}_{34}(\tilde{a})$ is depicted by the blue dashed/solid line. The inset in FIG. 11(a) demonstrates that for $\tilde{a} \leq \tilde{a}_1 \simeq 0.02$, the critical line is $\tilde{Q}_{12}(\tilde{a})$, on which black holes are RN type. Moreover, the critical line of iBI-AdS black holes in the \tilde{a} - \tilde{Q} plane is semi-infinite while that of BI-AdS black holes is a finite line. According to FIGs. 8(b) and 9(b), the critical line is physical since it globally minimizes the Gibbs free energy.

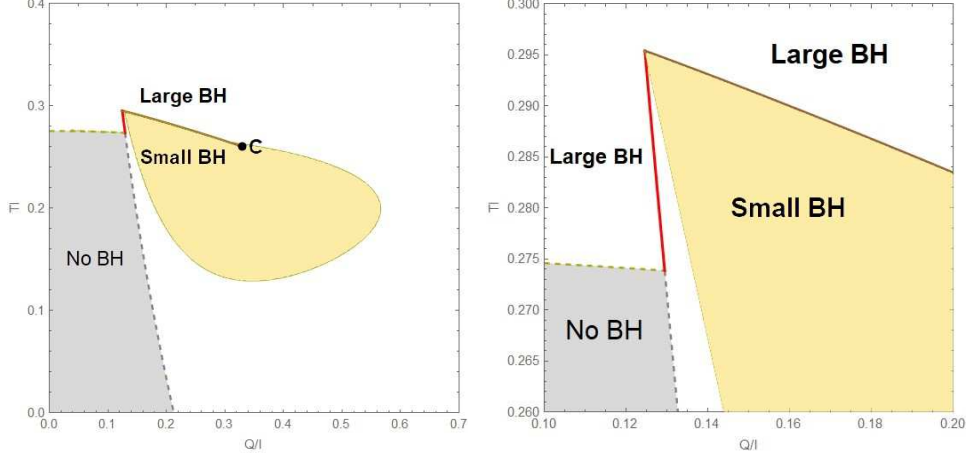
In the case of varying P with fixed values of Q and a , the system moves along $\tilde{Q}_l(\tilde{a}) = (Q/\sqrt{a})\sqrt{\tilde{a}}$ in the \tilde{a} - \tilde{Q} plane, which are plotted for various values of Q/\sqrt{a} in FIG. 11. FIG. 11(a) shows that there always exists one physical critical point. For $Q/\sqrt{a} \leq \tilde{Q}_1 \simeq 2.28$, the inset in FIG. 11(a) shows that the critical point occurs for the RN type black hole.

The boundary $\tilde{Q}_{45}(\tilde{a})$ is displayed by the red line in FIG. 11. If $\tilde{Q}_l(\tilde{a})$ intersects with $\tilde{Q}_{45}(\tilde{a})$, the black holes on $\tilde{Q}_l(\tilde{a})$ could be in Region V for some range of P . The numerical result and FIG. 11(b) show that when $Q/\sqrt{a} < 2$, $\tilde{Q}_l(\tilde{a})$ always intersects with $\tilde{Q}_{45}(\tilde{a})$, and there is a reentrant phase transition occurring for some range of P . Thus for $Q/\sqrt{a} < 2$, as P continuously increases from $P = 0$, the black holes on $\tilde{Q}_l(\tilde{a})$ experience the following regions: Region VI (no phase transitions) \rightarrow Region V (the LBH/SBH/LBH reentrant phase transition) \rightarrow Regions II or IV (the LBH/SBH first order phase transition) \rightarrow Regions I or III (no phase transitions). For $Q/\sqrt{a} > 2$, there is a critical point on $\tilde{Q}_l(\tilde{a})$ occurring at $P = P_c$. For $P < P_c$, the black holes on $\tilde{Q}_l(\tilde{a})$ with $Q/\sqrt{a} > 2$ are in Regions II or IV, and there is a first order phase transition between small BH and large BH. For $P > P_c$, they are in Regions I or III, and no phase transition occurs.

In the case of varying Q with fixed values of P and a , the system moves along a constant- \tilde{a} line in the \tilde{a} - \tilde{Q} plane. FIG. 11(a) shows that constant- \tilde{a} lines always intersect the critical line and the boundary $\tilde{Q}_{45}(\tilde{a})$. As one increases Q from $Q = 0$, the black holes on a constant- \tilde{a} line experience the following regions: Region VI (no phase transitions) \rightarrow Region V (the LBH/SBH/LBH reentrant phase transition) \rightarrow Regions II or IV (the LBH/SBH first order phase transition) \rightarrow Regions I or III (no phase transitions). For $\tilde{a} \geq 1/6$, the black holes on a constant- \tilde{a} line are always Schwarzschild-like type.

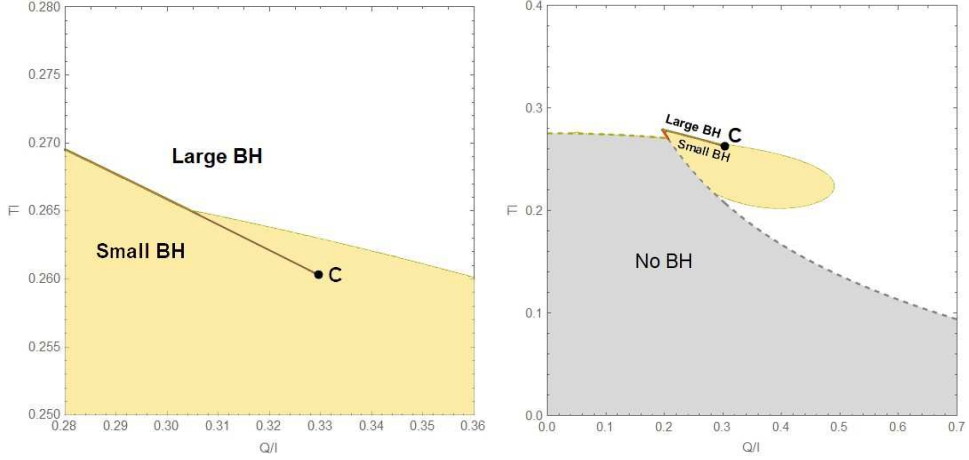
The phase diagrams of iBI-AdS black holes for $a/l^2 = 0.01$ and $a/l^2 = 0.1$ are displayed in the \tilde{Q} - \tilde{T} plane in FIG. 12, where we have the LBH/SBH first order phase transition lines (the brown lines), the LBH/SBH zeroth order phase transition lines (the red lines) and the critical points (the black dots). For $a/l^2 = 0.01$, FIGS. 6 and 12(a) shows that the phase diagram of iBI-AdS black holes is similar to that of BI-AdS black holes. Moreover, FIG. 12(d) shows that the phase diagram of iBI-AdS black holes with $a/l^2 = 0.1$ is similar to that with $a/l^2 = 0.01$, in the way that they have the LBH/SBH first order and the zeroth order phase transitions. This is expected from FIG. 11(a), which shows that the $a/l^2 = 0.1$ line intersects the critical line and the boundary $\tilde{Q}_{45}(\tilde{a})$. However, as shown in FIG. 7, there no phase transitions occurring in the phase diagram of BI-AdS black holes with $a/l^2 = 0.1$.

All phases in FIG. 12 are thermally stable. The black holes in the yellow region are electrically unstable. As with the critical points of BI-AdS black holes, the critical points of iBI-AdS black holes are also electrically unstable, which are highlighted in FIG. 12(c). For BI-AdS black holes, FIGS. 6 and 7 shows that the black holes very close to the boundaries of



(a) The phase diagram for $a/l^2 = 0.01$. (b) Highlighted region of the reentrant phase

transition in the phase diagram for $a/l^2 = 0.01$.



(c) Highlighted region near the critical point in (d) The phase diagram for $a/l^2 = 0.1$.

the phase diagram for $a/l^2 = 0.01$.

FIG. 12: The phase diagrams in the $\tilde{Q}-\tilde{T}$ plane for iBI-AdS black holes with $a/l^2 = 0.01$ in $a/l^2 = 0.1$. The first order phase transition lines separating large BH and small BH are displayed by the brown lines, and they terminate at the critical points, marked by black dots. There are also zeroth order phase transition lines, depicted by the red lines. All phases in the diagram are thermally stable. However, the phases in the yellow region are electrically unstable.

NO BH regions are always electrically unstable. However for iBI-AdS black holes, FIG. 12 shows that the black holes very close to the boundaries of NO BH regions can be electrically stable for large enough values of Q/l .

V. CONCLUSION

We have investigated the thermodynamic behavior of NLED AdS black holes in an extended phase space, which includes the conjugate pressure/volume quantities, any dimensionful couplings a_i in NLED and their associated conjugates \mathcal{A}_i . For a generic NLED black hole, we first computed its Euclidean action to obtain the Gibbs free energy. To obtain consistency of the Smarr relation, we found that it is necessary to include the conjugate pairs (a_i, \mathcal{A}_i) . It showed that the black hole's temperature T , charge Q , horizon radius r_+ (thermodynamic volume V), the AdS radius l (pressure P) and the dimensionful couplings a_i could be connected by

$$Tl = \tilde{T}(r_+/l, Q/l, a_i l^{-c_i}), \quad (74)$$

where c_i is the dimension of a_i . In the canonical ensemble with fixed T and Q , we found that the critical behavior and phase structure of the black hole are determined by $\tilde{Q} \equiv Q/l$ and $\tilde{a}_i \equiv a_i l^{-c_i}$.

For BI-AdS black holes, we examined their critical behavior and phase structure, whose dependence on \tilde{Q} and \tilde{a} was plotted in FIG. 4. There are six regions in FIG. 4, and each region has a different phase behavior. Specially, the LBH/SBH/LBH reentrant phase transition occurs in Region IV. For iBI-AdS black holes, we displayed the dependence of their critical behavior and phase structure on \tilde{Q} and \tilde{a} in FIG. 10, where there are also six regions, and the LBH/SBH/LBH reentrant phase transition occurs in Region V. We summarize the results of the critical behavior and phase structure for BI-AdS and iBI-AdS black holes in Table II.

The thermodynamically preferred phases, along with the zeroth and first phase transitions and critical points, were displayed in FIGs. 6 and 7 for BI-AdS black holes and in FIG. 12 for iBI-AdS black holes. We examined thermal and electrical stabilities of the black holes and found that all the thermodynamically preferred phases are thermal stable. However, the thermodynamically preferred phases in yellow regions in these figures were found to be electrical unstable. The possible equilibrium phases residing in the yellow regions were discussed in [9], which listed extremal black holes, anti-de Sitter space and black holes surrounded by a gas of particles as candidates. However, this question still remains open. In [49, 50, 61], the electrical transport behavior of the dual theory has been discussed for BI-AdS and iBI-AdS black holes in the context of gauge/gravity duality. It might be inspiring

	BI-AdS BH	iBI-AdS BH
Critical line	The critical line has a physical branch and an unphysical one, which have finite length and both terminate at $\{\tilde{a}_c, \tilde{Q}_c\} \simeq \{0.069, 0.37\}$.	The critical line is a semi-infinite line and extends to the infinity $\tilde{Q} = +\infty$.
Reentrant phase transition region	This region has a finite area and terminates at $\{\tilde{a}_c, \tilde{Q}_c\}$.	This region extends to the infinity $\tilde{Q} = +\infty$.
Varying P with fixed Q and a case ($\tilde{Q}_l(\tilde{a})$ line)	There exists one physical critical point for $Q/\sqrt{a} > \sqrt{2}$. The reentrant phase transition occurs for $\sqrt{2} < Q/\sqrt{a} < 2$.	There always exists one physical critical point. The reentrant phase transition occurs for $Q/\sqrt{a} < 2$.
Varying Q with fixed P and a case (constant- \tilde{a} line)	A physical critical point and reentrant phase transition occur for $\tilde{a} < \tilde{a}_c$.	A physical critical point and reentrant phase transition occur for all values of l and a .

TABLE II: Critical behavior and phase structure for BI-AdS and iBI-AdS black holes.

to explore the possible equilibrium phases residing in yellow regions from a holographic perspective.

Acknowledgments

We are grateful to Zheng Sun and Zhipeng Zhang for useful discussions and valuable comments. This work is supported in part by NSFC (Grant No. 11005016, 11175039 and 11375121).

Appendix A: Derivation of Smarr Relation

In this appendix, we directly derive the Smarr relation from the definitions of the thermodynamic quantities of the black hole. The Lagrangian $\mathcal{L}(s, a_i)$ is a function of s and the parameters a_i . Performing the dimensional analysis, we find

$$[\mathcal{L}] = L^{-2}, [s] = L^{-2}, [a_i] = L^{c_i}. \quad (\text{A1})$$

Euler's theorem says

$$2\mathcal{L}(s, a_i) = 2s\mathcal{L}'(s, a_i) - c_i a_i \frac{\partial \mathcal{L}(s, a_i)}{\partial a_i}. \quad (\text{A2})$$

For a dimensionful coupling a_i , we have

$$\begin{aligned} c_i a_i \mathcal{A}_i &= -4\pi c_i a_i \frac{\partial}{\partial a_i} \int_{r_+}^{\infty} dr r^2 \mathcal{L} \left(\frac{A_t'^2(r)}{2}, a_i \right) + c_i a_i Q \frac{\partial \Phi}{\partial a_i} \\ &= -c_i a_i \left[Q \frac{\partial \Phi}{\partial a_i} + 4\pi \int_{r_+}^{\infty} dr r^2 \frac{\partial \mathcal{L} \left(\frac{A_t'^2(r)}{2}, a_i \right)}{\partial a_i} \right] + c_i a_i Q \frac{\partial \Phi}{\partial a_i} \\ &= 8\pi \int_{r_+}^{\infty} dr r^2 \left[\mathcal{L} \left(\frac{A_t'^2(r)}{2}, a_i \right) - \frac{A_t'^2(r)}{2} \frac{\partial \mathcal{L} \left(\frac{A_t'^2(r)}{2}, a_i \right)}{\partial s} \right] \\ &= 8\pi \int_{r_+}^{\infty} dr r^2 \mathcal{L} \left(\frac{A_t'^2(r)}{2}, a_i \right) - Q\Phi. \end{aligned} \quad (\text{A3})$$

Therefore, one has

$$\begin{aligned} &2(TS - VP) + c_i a_i \mathcal{A}_i + Q\Phi \\ &= 8\pi r_+ \left\{ 1 + \frac{r_+^2}{l^2} + \frac{r_+^2}{2} \left[\mathcal{L} \left(\frac{A_t'^2(r_+)}{2}, a_i \right) - A_t'(r_+) \frac{Q}{r_+^2} \right] \right\} + 8\pi \int_{r_+}^{\infty} dr r^2 \mathcal{L}(s, a_i) \\ &= M - Q\Phi + 8\pi \left\{ \frac{3}{2} \int_{r_+}^{\infty} dr r^2 \mathcal{L} \left(\frac{A_t'^2(r)}{2}, a_i \right) + \frac{r_+^3}{2} \left[\mathcal{L} \left(\frac{A_t'^2(r_+)}{2}, a_i \right) - A_t'(r_+) \frac{Q\Phi}{r_+^2} \right] \right\} \\ &= M, \end{aligned}$$

where in the last equation, we use

$$\begin{aligned} \int_{r_+}^{\infty} dr r^2 \mathcal{L} \left(\frac{A_t'^2(r)}{2}, a_i \right) &= -\frac{r_+^3 \mathcal{L} \left(\frac{A_t'^2(r_+)}{2}, a_i \right)}{3} - \frac{1}{3} \int_{r_+}^{\infty} dr r^3 \mathcal{L}' \left(\frac{A_t'^2(r)}{2}, a_i \right) A_t'(r) A_t''(r) \\ &= -\frac{r_+^3 \mathcal{L}(s)}{3} + \frac{q}{3} A_t'(r_+) r_+ + \frac{q\Phi}{12\pi}. \end{aligned}$$

-
- [1] S. W. Hawking, "Particle Creation by Black Holes," *Commun. Math. Phys.* **43**, 199 (1975) Erratum: [*Commun. Math. Phys.* **46**, 206 (1976)]. doi:10.1007/BF02345020, 10.1007/BF01608497
- [2] J. D. Bekenstein, "Black holes and the second law," *Lett. Nuovo Cim.* **4**, 737 (1972). doi:10.1007/BF02757029

- [3] J. D. Bekenstein, “Black holes and entropy,” *Phys. Rev. D* **7**, 2333 (1973). doi:10.1103/PhysRevD.7.2333
- [4] J. M. Bardeen, B. Carter and S. W. Hawking, “The Four laws of black hole mechanics,” *Commun. Math. Phys.* **31**, 161 (1973). doi:10.1007/BF01645742
- [5] J. M. Maldacena, “The Large N limit of superconformal field theories and supergravity,” *Int. J. Theor. Phys.* **38**, 1113 (1999) [*Adv. Theor. Math. Phys.* **2**, 231 (1998)] doi:10.1023/A:1026654312961, 10.4310/ATMP.1998.v2.n2.a1 [hep-th/9711200].
- [6] S. W. Hawking and D. N. Page, “Thermodynamics of Black Holes in anti-De Sitter Space,” *Commun. Math. Phys.* **87**, 577 (1983). doi:10.1007/BF01208266
- [7] E. Witten, “Anti-de Sitter space, thermal phase transition, and confinement in gauge theories,” *Adv. Theor. Math. Phys.* **2**, 505 (1998) doi:10.4310/ATMP.1998.v2.n3.a3 [hep-th/9803131].
- [8] A. Chamblin, R. Emparan, C. V. Johnson and R. C. Myers, “Charged AdS black holes and catastrophic holography,” *Phys. Rev. D* **60**, 064018 (1999) doi:10.1103/PhysRevD.60.064018 [hep-th/9902170].
- [9] A. Chamblin, R. Emparan, C. V. Johnson and R. C. Myers, “Holography, thermodynamics and fluctuations of charged AdS black holes,” *Phys. Rev. D* **60**, 104026 (1999) doi:10.1103/PhysRevD.60.104026 [hep-th/9904197].
- [10] B. P. Dolan, “Pressure and volume in the first law of black hole thermodynamics,” *Class. Quant. Grav.* **28**, 235017 (2011) doi:10.1088/0264-9381/28/23/235017 [arXiv:1106.6260 [gr-qc]].
- [11] D. Kubiznak and R. B. Mann, “P-V criticality of charged AdS black holes,” *JHEP* **1207**, 033 (2012) doi:10.1007/JHEP07(2012)033 [arXiv:1205.0559 [hep-th]].
- [12] D. Kastor, S. Ray and J. Traschen, “Enthalpy and the Mechanics of AdS Black Holes,” *Class. Quant. Grav.* **26**, 195011 (2009) doi:10.1088/0264-9381/26/19/195011 [arXiv:0904.2765 [hep-th]].
- [13] S. W. Wei and Y. X. Liu, “Critical phenomena and thermodynamic geometry of charged Gauss-Bonnet AdS black holes,” *Phys. Rev. D* **87**, no. 4, 044014 (2013) doi:10.1103/PhysRevD.87.044014 [arXiv:1209.1707 [gr-qc]].
- [14] R. G. Cai, L. M. Cao, L. Li and R. Q. Yang, “P-V criticality in the extended phase space of Gauss-Bonnet black holes in AdS space,” *JHEP* **1309**, 005 (2013) doi:10.1007/JHEP09(2013)005 [arXiv:1306.6233 [gr-qc]].

- [15] W. Xu and L. Zhao, “Critical phenomena of static charged AdS black holes in conformal gravity,” *Phys. Lett. B* **736**, 214 (2014) doi:10.1016/j.physletb.2014.07.019 [arXiv:1405.7665 [gr-qc]].
- [16] A. M. Frassino, D. Kubiznak, R. B. Mann and F. Simovic, “Multiple Reentrant Phase Transitions and Triple Points in Lovelock Thermodynamics,” *JHEP* **1409**, 080 (2014) doi:10.1007/JHEP09(2014)080 [arXiv:1406.7015 [hep-th]].
- [17] M. H. Dehghani, S. Kamrani and A. Sheykhi, “ $P - V$ criticality of charged dilatonic black holes,” *Phys. Rev. D* **90**, no. 10, 104020 (2014) doi:10.1103/PhysRevD.90.104020 [arXiv:1505.02386 [hep-th]].
- [18] R. A. Hennigar, W. G. Brenna and R. B. Mann, “ $P?v$ criticality in quasitopological gravity,” *JHEP* **1507**, 077 (2015) doi:10.1007/JHEP07(2015)077 [arXiv:1505.05517 [hep-th]].
- [19] S. Gunasekaran, R. B. Mann and D. Kubiznak, “Extended phase space thermodynamics for charged and rotating black holes and Born-Infeld vacuum polarization,” *JHEP* **1211**, 110 (2012) doi:10.1007/JHEP11(2012)110 [arXiv:1208.6251 [hep-th]].
- [20] N. Altamirano, D. Kubiznak and R. B. Mann, “Reentrant phase transitions in rotating anti-de Sitter black holes,” *Phys. Rev. D* **88**, no. 10, 101502 (2013) doi:10.1103/PhysRevD.88.101502 [arXiv:1306.5756 [hep-th]].
- [21] D. C. Zou, R. Yue and M. Zhang, “Reentrant phase transitions of higher-dimensional AdS black holes in dRGT massive gravity,” *Eur. Phys. J. C* **77**, no. 4, 256 (2017) doi:10.1140/epjc/s10052-017-4822-9 [arXiv:1612.08056 [gr-qc]].
- [22] R. A. Hennigar and R. B. Mann, “Reentrant phase transitions and van der Waals behaviour for hairy black holes,” *Entropy* **17**, no. 12, 8056 (2015) doi:10.3390/e17127862 [arXiv:1509.06798 [hep-th]].
- [23] H. H. Soleng, “Charged black points in general relativity coupled to the logarithmic U(1) gauge theory,” *Phys. Rev. D* **52**, 6178 (1995) doi:10.1103/PhysRevD.52.6178 [hep-th/9509033].
- [24] E. Ayon-Beato and A. Garcia, “Regular black hole in general relativity coupled to nonlinear electrodynamics,” *Phys. Rev. Lett.* **80**, 5056 (1998) doi:10.1103/PhysRevLett.80.5056 [gr-qc/9911046].
- [25] H. Maeda, M. Hassaine and C. Martinez, “Lovelock black holes with a nonlinear Maxwell field,” *Phys. Rev. D* **79**, 044012 (2009) doi:10.1103/PhysRevD.79.044012 [arXiv:0812.2038 [gr-qc]].

- [26] S. H. Hendi, B. Eslam Panah, S. Panahiyan and A. Sheykhi, “Dilatonic BTZ black holes with power-law field,” *Phys. Lett. B* **767**, 214 (2017) doi:10.1016/j.physletb.2017.01.066 [arXiv:1703.03403 [gr-qc]].
- [27] J. Tao, P. Wang and H. Yang, “Testing holographic conjectures of complexity with Born–Infeld black holes,” *Eur. Phys. J. C* **77**, no. 12, 817 (2017) doi:10.1140/epjc/s10052-017-5395-3 [arXiv:1703.06297 [hep-th]].
- [28] X. Guo, P. Wang and H. Yang, “Membrane Paradigm and Holographic DC Conductivity for Nonlinear Electrodynamics,” *Phys. Rev. D* **98**, no. 2, 026021 (2018) doi:10.1103/PhysRevD.98.026021 [arXiv:1711.03298 [hep-th]].
- [29] B. Mu, P. Wang and H. Yang, “Holographic DC Conductivity for a Power-law Maxwell Field,” arXiv:1711.06569 [hep-th].
- [30] S. H. Hendi and M. H. Vahidinia, “Extended phase space thermodynamics and P-V criticality of black holes with a nonlinear source,” *Phys. Rev. D* **88**, no. 8, 084045 (2013) doi:10.1103/PhysRevD.88.084045 [arXiv:1212.6128 [hep-th]].
- [31] J. X. Mo, G. Q. Li and X. B. Xu, “Effects of power-law Maxwell field on the critical phenomena of higher dimensional dilaton black holes,” *Phys. Rev. D* **93**, no. 8, 084041 (2016) doi:10.1103/PhysRevD.93.084041 [arXiv:1601.05500 [gr-qc]].
- [32] P. K. Yerra and C. Bhamidipati, “A Note on Critical Nonlinearly Charged Black Holes,” arXiv:1806.08226 [hep-th].
- [33] C. H. Nam, “Non-linear charged dS black hole and its thermodynamics and phase transitions,” *Eur. Phys. J. C* **78**, no. 5, 418 (2018). doi:10.1140/epjc/s10052-018-5922-x
- [34] T. K. Dey, “Born-Infeld black holes in the presence of a cosmological constant,” *Phys. Lett. B* **595**, 484 (2004) doi:10.1016/j.physletb.2004.06.047 [hep-th/0406169].
- [35] R. G. Cai, D. W. Pang and A. Wang, “Born-Infeld black holes in (A)dS spaces,” *Phys. Rev. D* **70**, 124034 (2004) doi:10.1103/PhysRevD.70.124034 [hep-th/0410158].
- [36] S. Fernando and D. Krug, “Charged black hole solutions in Einstein-Born-Infeld gravity with a cosmological constant,” *Gen. Rel. Grav.* **35**, 129 (2003) doi:10.1023/A:1021315214180 [hep-th/0306120].
- [37] S. Fernando, “Thermodynamics of Born-Infeld-anti-de Sitter black holes in the grand canonical ensemble,” *Phys. Rev. D* **74**, 104032 (2006) doi:10.1103/PhysRevD.74.104032 [hep-th/0608040].

- [38] R. Banerjee, S. Ghosh and D. Roychowdhury, “New type of phase transition in Reissner Nordstrom–AdS black hole and its thermodynamic geometry,” *Phys. Lett. B* **696**, 156 (2011) doi:10.1016/j.physletb.2010.12.010 [arXiv:1008.2644 [gr-qc]].
- [39] R. Banerjee and D. Roychowdhury, “Critical phenomena in Born-Infeld AdS black holes,” *Phys. Rev. D* **85**, 044040 (2012) doi:10.1103/PhysRevD.85.044040 [arXiv:1111.0147 [gr-qc]].
- [40] A. Lala and D. Roychowdhury, “Ehrenfest’s scheme and thermodynamic geometry in Born-Infeld AdS black holes,” *Phys. Rev. D* **86**, 084027 (2012) doi:10.1103/PhysRevD.86.084027 [arXiv:1111.5991 [gr-qc]].
- [41] R. Banerjee and D. Roychowdhury, “Critical behavior of Born Infeld AdS black holes in higher dimensions,” *Phys. Rev. D* **85**, 104043 (2012) doi:10.1103/PhysRevD.85.104043 [arXiv:1203.0118 [gr-qc]].
- [42] M. Azreg-Ainou, “Black hole thermodynamics: No inconsistency via the inclusion of the missing $P - V$ terms,” *Phys. Rev. D* **91**, 064049 (2015) doi:10.1103/PhysRevD.91.064049 [arXiv:1411.2386 [gr-qc]].
- [43] S. H. Hendi, B. Eslam Panah and S. Panahiyan, “Einstein-Born-Infeld-Massive Gravity: adS-Black Hole Solutions and their Thermodynamical properties,” *JHEP* **1511**, 157 (2015) doi:10.1007/JHEP11(2015)157 [arXiv:1508.01311 [hep-th]].
- [44] M. Kord Zangeneh, A. Dehyadegari, M. R. Mehdizadeh, B. Wang and A. Sheykhi, “Thermodynamics, phase transitions and Ruppeiner geometry for Einstein–dilaton–Lifshitz black holes in the presence of Maxwell and Born–Infeld electrodynamics,” *Eur. Phys. J. C* **77**, no. 6, 423 (2017) doi:10.1140/epjc/s10052-017-4989-0 [arXiv:1610.06352 [hep-th]].
- [45] X. X. Zeng, X. M. Liu and L. F. Li, “Phase structure of the Born–Infeld–anti-de Sitter black holes probed by non-local observables,” *Eur. Phys. J. C* **76**, no. 11, 616 (2016) doi:10.1140/epjc/s10052-016-4463-4 [arXiv:1601.01160 [hep-th]].
- [46] S. Li, H. Lu and H. Wei, “Dyonic (A)dS Black Holes in Einstein-Born-Infeld Theory in Diverse Dimensions,” *JHEP* **1607**, 004 (2016) doi:10.1007/JHEP07(2016)004 [arXiv:1606.02733 [hep-th]].
- [47] D. C. Zou, S. J. Zhang and B. Wang, “Critical behavior of Born-Infeld AdS black holes in the extended phase space thermodynamics,” *Phys. Rev. D* **89**, no. 4, 044002 (2014) doi:10.1103/PhysRevD.89.044002 [arXiv:1311.7299 [hep-th]].
- [48] A. Dehyadegari and A. Sheykhi, “Reentrant phase transition of Born-Infeld-AdS black holes,”

- Phys. Rev. D **98**, no. 2, 024011 (2018) doi:10.1103/PhysRevD.98.024011 [arXiv:1711.01151 [gr-qc]].
- [49] M. Baggioli and O. Pujolas, “On Effective Holographic Mott Insulators,” JHEP **1612**, 107 (2016) doi:10.1007/JHEP12(2016)107 [arXiv:1604.08915 [hep-th]].
- [50] P. Wang, H. Wu and H. Yang, “Holographic DC Conductivity for Backreacted Nonlinear Electrodynamics with Momentum Dissipation,” arXiv:1805.07913 [hep-th].
- [51] S. W. Hawking, “Quantum Gravity and Path Integrals,” Phys. Rev. D **18**, 1747 (1978). doi:10.1103/PhysRevD.18.1747
- [52] G. Gibbons, “Euclidean quantum gravity: The view from 2002,” in The Future of Theoretical Physics and Cosmology.
- [53] A. Chamblin, R. Emparan, C. V. Johnson and R. C. Myers, “Holography, thermodynamics and fluctuations of charged AdS black holes,” Phys. Rev. D **60**, 104026 (1999) doi:10.1103/PhysRevD.60.104026 [hep-th/9904197].
- [54] V. Balasubramanian and P. Kraus, “A Stress tensor for Anti-de Sitter gravity,” Commun. Math. Phys. **208**, 413 (1999) doi:10.1007/s002200050764 [hep-th/9902121].
- [55] R. Emparan, C. V. Johnson and R. C. Myers, “Surface terms as counterterms in the AdS / CFT correspondence,” Phys. Rev. D **60**, 104001 (1999) doi:10.1103/PhysRevD.60.104001 [hep-th/9903238].
- [56] R. Olea, “Mass, angular momentum and thermodynamics in four-dimensional Kerr-AdS black holes,” JHEP **0506**, 023 (2005) doi:10.1088/1126-6708/2005/06/023 [hep-th/0504233].
- [57] R. Olea, “Regularization of odd-dimensional AdS gravity: Kounterterms,” JHEP **0704**, 073 (2007) doi:10.1088/1126-6708/2007/04/073 [hep-th/0610230].
- [58] O. Miskovic and R. Olea, “Thermodynamics of Einstein-Born-Infeld black holes with negative cosmological constant,” Phys. Rev. D **77**, 124048 (2008) doi:10.1103/PhysRevD.77.124048 [arXiv:0802.2081 [hep-th]].
- [59] D. Kastor, S. Ray and J. Traschen, “Smarr Formula and an Extended First Law for Lovelock Gravity,” Class. Quant. Grav. **27**, 235014 (2010) doi:10.1088/0264-9381/27/23/235014 [arXiv:1005.5053 [hep-th]].
- [60] D. Kastor, S. Ray and J. Traschen, “Enthalpy and the Mechanics of AdS Black Holes,” Class. Quant. Grav. **26**, 195011 (2009) doi:10.1088/0264-9381/26/19/195011 [arXiv:0904.2765 [hep-th]].

- [61] S. Cremonini, A. Hoover and L. Li, “Backreacted DBI Magnetotransport with Momentum Dissipation,” *JHEP* **1710**, 133 (2017) doi:10.1007/JHEP10(2017)133 [arXiv:1707.01505 [hep-th]].